ELSEVIER

Contents lists available at ScienceDirect

# Results in Control and Optimization

journal homepage: www.elsevier.com/locate/rico





# Modeling environmental-born melioidosis dynamics with recurrence: An application of optimal control

Habtamu Ayalew Engida

Department of Applied Mathematics, Debre Markos University, Debre Markos, P.O. Box 269, Ethiopia

# ARTICLE INFO

Keywords:
Melioidosis model
B.pseudomallei
Recurrent
Global stability
Optimal control
Cost-effective strategy

#### ABSTRACT

Melioidosis is a significant health problem in tropical and subtropical regions, especially in Southeast Asia and Northern Australia. Recurrent melioidosis is a major obstacle to eliminating the disease from the community in these nations. This work aims to propose and analyze a human melioidosis model with recurrent phenomena and an optimal control model by incorporating time-dependent control functions. The basic reproduction number  $(R_0)$  of the uncontrolled model is derived using the method of the next-generation matrix. Using the construction of a Lyapunov functional, we present the global asymptotic dynamics of the autonomous model in the presence of recurrent for both disease-free and endemic equilibria. The global asymptotic stability of the model's equilibria shows the absence of a backward bifurcation for the model in both cases, whether in the absence or presence of relapse. The sensitivity analysis aims to identify the parameters that have the most significant impact on the model's dynamics. Furthermore, qualitative analysis of the model's global dynamics and the changing effect of the most influential parameters on  $R_0$  are supported by numerical experiments, with the results being illustrated graphically. The model with time-dependent controls is analyzed using optimal control theory to assess the impact of various intervention strategies on the spread of the epidemic. The numerical results of the optimality system are carried out using the Forward-Backward Sweep method in Matlab. We also conducted a cost-effectiveness analysis using two approaches: the average cost-effectiveness ratio and the incremental cost-effectiveness ratio.

#### 1. Introduction

Melioidosis is an infectious disease caused by the facultative intracellular gram-negative bacterium *Burkholderia pseudomallei* (*B. pseudomallei*). The environment (wet soil and surface water) is the natural reservoir of the pathogen in certain regions of the world where the disease is prevalent [1,2]. The organism is endemic in Southeast Asia and Northern Australia and is becoming a significant emerging infection in other tropical and subtropical regions of the world, such as India, China, Sub-Saharan Africa, and Central and South America [3,4]. Recent studies have estimated that there are about 165,000 human melioidosis cases annually worldwide, with 89,000 (54%) fatalities [5,6]. Humans acquire *B.pseudomallei* infections through contact with a contaminated environment (soil or water) via percutaneous inoculation, inhalation, or ingestion [7–9]. Human-to-human transmission has been reported as extremely rare, with only a few suspected cases documented to date [10,11]. Melioidosis is a severe human infection, which can manifest as acute, chronic, or recurrent, with a mortality rate ranging from 10–50% [12,13]. Subsequent studies have shown that the recurrence of the disease occurs from 5.7–25% in patients, depending on the geographical area. Recurrence of melioidosis is commonly reported in endemic areas, and can be classified as either a relapse or a reinfection [14,15]. Relapse involves the reappearance of *B. pseudomallei* infection with the same genotype as the original infection, accounting for 74–75% of

E-mail address: hayalew\_engida@dmu.edu.et.

https://doi.org/10.1016/j.rico.2024.100476

Received 8 May 2024; Received in revised form 6 June 2024; Accepted 10 September 2024

Available online 12 September 2024

2666-7207/© 2024 The Author. Published by Elsevier B.V. This is an open access article under the CC BY-NC-ND license (http://creativecommons.org/licenses/by-nc-nd/4.0/).

all recurrences [16,17]. On the other hand, reinfection is the emergence of a new infection with a different genotype from that of the original infection, and it ranges from 25–26% of all recurrences [18,19]. Patients with mild illness can be treated through intravenous antibiotics involving ceftazidime, imipenem, carbapenem, cefepime or meropenem [20,21]. In fact, *B. pseudomallei* species are inherently resistant to multiple classes of antimicrobial agents [22,23]. Recent studies have reported that treatments such as trimethoprim–sulfamethoxazole (TMP–SMX) for 140 days, TMP–SMX plus doxycycline for more than 3 months, or TMP–SMX plus doxycycline plus chloramphenicol for more than 12 weeks are currently recommended to prevent severe and relapse melioidosis [24–26].

Many fields including mathematical biology, epidemiology, engineering, and economics require applying applied mathematics to describe various phenomena mathematically [27]. Specifically, mathematical modeling is a powerful tool for studying infectious diseases. It helps to understand and predict disease spread, and optimize control interventions using optimal control theory. The optimal control theory is vital in designing better health measures for a specific mathematical model to control and eventually eliminate diseases [28–30].

A few deterministic mathematical models have been proposed in various forms to study the transmission dynamics of melioidosis in the absence of optimal controls. In [31], the authors developed a melioidosis model under the assumption that the recovered individuals either return to the latently infected (exposed) class (re-infection) or to the infectious class (relapse), but they considered one recovered class (without separating relapse and re-infection in their model). They showed the existence of backward bifurcation in the presence of disease recurrence. They also considered both human-to-human and environment-to-human transmission paths in the transmission dynamics of the diseases.

The authors in [32] presented a mathematical model of melioidosis dynamics with the assumption that the latently-infected humans progress to either symptomatic class (infectious individuals that are showing symptoms) or to asymptomatic (infectious individuals without symptoms). Meanwhile, the author in [33] proposed a deterministic model to achieve the effectiveness of two control measures on the transmission dynamics of melioidosis using optimal control theory. They considered a single transmission way, mass action incidence rate (homogeneous interaction) for interaction between susceptible humans and contaminated environment. Likewise, the authors in [34] recently investigated a non-autonomous melioidosis model by applying optimal control theory, expanding on the research started in [32].

The global asymptotic dynamics of the melioidosis model and the impact of optimal control measures in the presence of disease recurrence have not been explored in the existing literature. Other existing disease models that did not consider the recurrence focused solely on the local stability of the model's steady states. Therefore, this crucial aspect is overlooked for environmental-born melioidosis in the population. Also, the existing melioidosis model with recurrent cases experiences backward bifurcation in the presence of disease recurrence [31]. In this work, we consider two distinct biological recurrences of melioidosis – relapse and reinfection – as separate classes. Thus, this study examines the global dynamic behavior of a robust melioidosis model in the presence of relapse and re-infection based on applications of the Lyapunov stability approach and optimal control theory with cost-effectiveness analysis. Thus, we aim to answer the following: (i) what will be the sufficient condition for the disease elimination? (ii) Is it possible to establish the absence of the phenomenon of backward bifurcation in the presence of reinfection and relapse? (iii) Is it possible to establish a result for global asymptotic stability of the existing disease-free equilibrium point in the presence of reinfection and relapse? (iv) what will be the sufficient condition for global asymptotic stability of the existing endemic equilibrium point in the presence of reinfection and relapse? (v) what will be the most effective control measures for disease elimination? (vi) what will be the most cost-effective strategy for disease control?

The rest of the paper is organized as follows: A compartmental model is formulated in Section 2. The basic qualitative properties of the model (non-negativity and boundedness of solutions) and the existence and stability of equilibria are presented in Section 3. Section 4 presents the sensitivity analysis of the basic reproduction number. The numerical simulations of the autonomous model are presented in Section 5. The formulation, theoretical analysis, numerical simulations, and cost-effectiveness analysis of the optimal control problem are provided in Section 6. Concluding remarks and future directions are given in Section 7.

# 2. Model formulation

The model proposed consists of human and the disease's pathogen populations. Based on the disease's epidemiological behaviors, the total human population at any time t, denoted by N(t), is divided into five distinct classes: susceptible S(t), infected individuals but not infectious (exposed) E(t), infectious individuals I(t), pseudo-recovered individuals with possible reactivation of infection (relapse) represented by  $R_1(t)$ , and  $R_2(t)$  denotes recovered individuals with possibility of reinfection. Thus, N(t) is given by

$$N(t) = S(t) + E(t) + I(t) + R_1(t) + R_2(t).$$
(2.1)

The pathogen population at time t is represented as P(t). Susceptible individuals are assumed to be recruited at a constant rate of  $\Lambda$ . The susceptible class could acquire the disease through percutaneous inoculation, inhalation, and ingestion of the pathogen from the contaminated environment at the rate

$$\Phi = \frac{\alpha P}{\kappa + P},\tag{2.2}$$

and progress to exposed class, where  $\alpha$  is transmission rate,  $\kappa$  is the constant pathogen concentration in the environment that yields 50% chance of catching melioidiosis, and a nonlinear expression  $\frac{P}{\kappa+P}$  denotes the contact probability between humans and contaminated environment. Hence, the number of infections per unit of time is given by  $\Phi S$ . The individuals in I move to either  $R_2$  with probability  $\tau$  or progress to  $R_1$  with probability  $1-\tau$ . After recovery from infection, an individual is not permanently immune

**Table 1** Descriptions and values of parameters of the model.

Parameter	Description	Value	Unit	Source
Λ	Human recruitment rate	$\mu \times N0$	Humans day <sup>-1</sup>	[31,32]
α	Transmission rate	0.0185	Day <sup>-1</sup>	Assumed
$\mu$	Natural death rate of humans	1 65×365	Day <sup>-1</sup>	[31]
$\theta$	Progression rate of E to I	<u>Y</u>	$Day^{-1}$	[32,33]
γ	Recovery rate	ó.0037	Day <sup>-1</sup>	[32,35]
δ	Disease-induced death rate	0.005	Day <sup>-1</sup>	[31,32]
$\eta_1$	Relapse rate of humans in $R_1$	0.069	Day <sup>-1</sup>	Assumed
$\eta_2$	Reduction rate of infectivity in $R_2$	0.035	Dimensionless	Assumed
σ	Rate at which bacteria increase by I	0.13	No. of B. pseudomalleicell Humans day	[33]
$\mu_b$	Natural mortality rate of pathogens	0.02	Day <sup>-1</sup>	[32,33]
κ	Concentration of B. pseudomallei	5000	No. of B. pseudomallei cell	Assumed

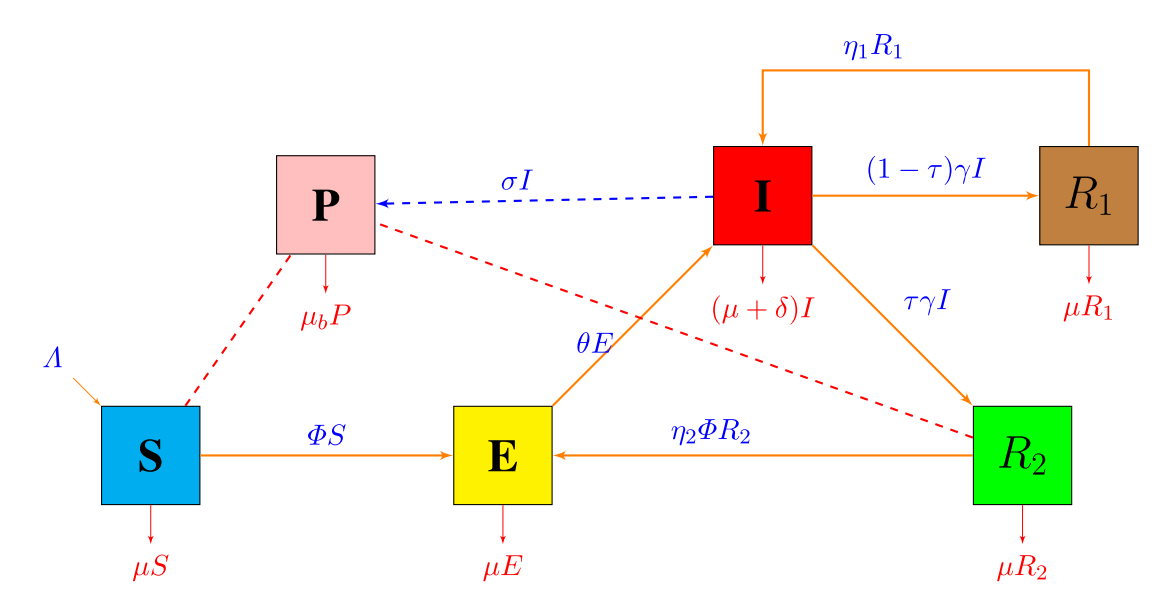


Fig. 1. Schematic diagram illustrating the dynamics of melioidosis with recurrence: The yellow bold arrow indicates the movement of individuals from one compartment to the other, the blue dotted arrow represents the contribution of the infectious class to the pathogen class, and the red dotted segment indicates the contribution to transmission. (For interpretation of the references to color in this figure legend, the reader is referred to the web version of this article.)

from *B.pseudomallei*, particularly due to recurrence (either relapse or reinfection). Thus, individuals in  $R_2$  class could acquire reinfection at the rate  $\eta_2\Phi$  and move to the exposed class, where,  $\eta_2\in[0,1]$  is the reduction in infectivity of  $R_2$ . Also, it is assumed that individuals in  $R_1$  class relapse at the rate  $\eta_1$ . Furthermore, the natural mortality rates of humans and the pathogen are represented by  $\mu$  and  $\mu_b$ , respectively. The size of class P grows in a contaminated environment due to the release of the pathogen from class I at a rate of  $\sigma$ .

Model's parameter descriptions and values are explained in Table 1.

Based on the model descriptions above, the compartmental melioidosis model with recurrence is shown in Fig. 1. According to Fig. 1, the melioidosis model takes the following system of non-linear ODEs:

For initial conditions and things.

Fig. 1, the inelabolicies model takes the following system of non-initial ODES.

$$\frac{dS}{dt} = \Lambda - \left(\frac{\alpha P}{\kappa + P} + \mu\right) S, \\
\frac{dE}{dt} = \frac{\alpha P}{\kappa + P} \left(S + \eta_2 R_2\right) - (\theta + \mu) E, \\
\frac{dI}{dt} = \theta E + \eta_1 R_1 - (\gamma + \delta + \mu) I, \\
\frac{dR_1}{dt} = (1 - \tau) \gamma I - (\eta_1 + \mu) R_1, \\
\frac{dR_2}{dt} = \tau \gamma I - \left(\mu + \eta_2 \frac{\alpha P}{\kappa + P}\right) R_2, \\
\frac{dP}{dt} = \sigma I - \mu_b P,$$
(2.3)

with the initial conditions;

$$S(0) \ge 0$$
,  $E(0) \ge 0$ ,  $I(0) \ge 0$ ,  $R_1(0) \ge 0$ ,  $R_2(0) \ge 0$ , and  $P(0) \ge 0$ .

#### 3. Model analysis

In this section, we qualitatively analyze the autonomous model (2.3).

#### 3.1. Basic properties of the model

#### 3.1.1. Non-negativity of the model solutions

For the model equation system (2.3) to be epidemiologically meaningful, it is crucial to demonstrate that all its state variables remain non-negative over time *t*.

**Theorem 3.1.** Let the set for the initial states be  $M_0 = \left(S(0), E(0), I(0), R_1(0), R_2(0), P(0)\right) \in R_+^6 \cup \{0\}$ . Then, the solutions  $\left\{S(t), E(t), I(t), R_1(t), R_2(t), P(t)\right\}$  of the model (2.3) are non-negative for all t > 0.

**Proof.** Let  $t_f = \sup\{t > 0 : S(t_0) > 0, E(t_0) > 0, I(t_0) > 0, R_1(t_0) > 0, R_2(t_0), P(t_0) > 0, \forall t_0 \text{ in } [0, t]\}$ . It follows that  $t_f > 0$ . From the 1st equation of the system (2.3) it follows that

$$\frac{dS}{dt} + (\Phi + \mu)S = \Lambda, \text{ where, } \Phi = \frac{\alpha P}{\kappa + P}.$$
 (3.1)

By applying the method of integrating factor on Eq. (3.1), we have

$$\frac{d}{dt}\left[S(t)e^{\mu t_f + \int_0^{t_f} \Phi(u)du}\right] = \Lambda e^{\mu t_f + \int_0^{t_f} \Phi(u)du}.$$
(3.2)

Integrating both sides of Eq. (3.2) yields,

$$S(t_f)e^{\mu t_f + \int_0^{t_f} \Phi(u)du} - S(0) = \int_0^{t_f} \Lambda \left[ e^{\mu v + \int_0^v \Phi(u)du} \right] dv.$$

Therefore,

$$S(t_f) = S(0)e^{-\mu t_f - \int_0^{t_f} \boldsymbol{\Phi}(u)du} + \left[e^{-\mu t_f - \int_0^{t_f} \boldsymbol{\Phi}(u)du}\right] \times \int_0^{t_f} \left[e^{\mu v + \int_0^v \boldsymbol{\Phi}(u)du}\boldsymbol{\Lambda}\right] dv \geq 0.$$

Also from the 5th equation of the system (2.3) it follows that

$$\frac{dR_2}{dt} \ge -\left(\mu + \eta_2 \frac{\alpha P}{\kappa + P}\right) R_2 \ge -\left(\mu + \eta_2 \alpha\right) R_2,\tag{3.3}$$

since the state variables and parameters are non-negative  $\frac{P}{\kappa+P} \le 1 \Rightarrow \left(\mu + \eta_2 \frac{\alpha P}{\kappa+P}\right) R_2 \le \left(\mu + \eta_2 \alpha\right) R_2$ . Thus, using integrating factor method and the comparison theorem given in [36] the inequality (3.3), yields

$$R_2(t) \ge R_2(0)e^{-(\mu+\eta_2\alpha)t} \ge 0, \forall t > 0.$$

In the same manner,

$$\begin{cases} \frac{dE}{dt} \geq -(\theta + \mu)E, & \Rightarrow E(t) \geq E(0)e^{-(\theta + \mu)t} \geq 0, \forall t > 0, \\ \frac{dI}{dt} \geq -(\gamma + \delta + \mu)I, & \Rightarrow I(t) \geq I(0)e^{-(\gamma + \delta + \mu)t} \geq 0, \forall t > 0, \\ \frac{dR_1}{dt} \geq -(\eta_1 + \mu)R_1, & \Rightarrow R_1(t) \geq R_1(0)e^{-(\eta_1 + \mu)t} \geq 0, \forall t > 0, \\ \frac{dP}{dt} \geq -\mu_b P, & \Rightarrow P(t) \geq P(0)e^{-\mu_b t} \geq 0, \forall t > 0. \end{cases}$$

Hence, the solutions of (2.3) with non-negative initial conditions  $M_0 \in \mathbb{R}^6_+ \cup \{0\}$  remain non-negative for all t > 0.

# 3.1.2. Boundedness of the model solutions

**Lemma 3.2.** The closed set  $D_1$  given by  $D_1 = \{(S, E, I, R_1, R_2, P) \in R_+^6 : 0 \le N(t) \le \frac{\Lambda}{\mu}, 0 \le P(t) \le \frac{\sigma \Lambda}{\mu \mu_b} \}$ , is positively invariant and attracts every positive solution of the model.

Proof. Adding all the first five equations of the system (2.3), yields

$$\frac{dN(t)}{dt} = \Lambda - \mu N(t) - \delta I(t). \tag{3.4}$$

Since  $\delta$  and I are non-negative, from Eq. (3.4), it follows that

$$\frac{dN(t)}{dt} \le \Lambda - \mu N(t), \text{ or } \frac{dN(t)}{dt} + \mu N(t) \le \Lambda, \ \forall t \ge 0.$$
(3.5)

Applying the integrating factor method and the comparison theorem [36] to Eq. (3.5), gives

$$N(t) \le \frac{\Lambda}{\mu} + \left(N(0) - \frac{\Lambda}{\mu}\right) e^{-\mu t}.$$
(3.6)

Thus,  $0 \le \lim_{t \to \infty} \sup N(t) \le \frac{\Lambda}{\mu}$ . In particular, if  $N(0) \le \frac{\Lambda}{\mu}$ , then  $N(t) \le \frac{\Lambda}{\mu}$ ,  $\forall t > 0$ . Furthermore, if  $N(0) > \frac{\Lambda}{\mu}$ , then either the solution enters the region  $D_1$  in finite time or  $N(t) \longrightarrow \frac{\Lambda}{\mu}$  asymptotically as  $t \to \infty$ . Lastly, using the last equation of (2.3), and the Eqs. (2.1) and (3.6), we obtain

$$P(t) \le \frac{\sigma \Lambda}{\mu_b \mu} + \left(P(0) - \frac{\sigma \Lambda}{\mu_b \mu}\right) e^{-\mu_b t}, \ \forall t > 0.$$

This implies that

$$0 \le \lim_{t \to \infty} \sup P(t) \le \frac{\sigma \Lambda}{\mu_b \mu}.$$

Therefore,  $0 \le P(t) \le \frac{\sigma \Lambda}{\mu_b \mu}$  whenever,  $0 \le P(0) \le \frac{\sigma \Lambda}{\mu_b \mu}$ ,  $\forall t > 0$ . Similarly,  $P(t) \longrightarrow \frac{\sigma \Lambda}{\mu_b \mu}$  asymptotically as  $t \to \infty$ . Consequently, the region  $D_1 \subset R_+^6$  is positively invariant and attracts all solutions of the system (2.3), it suffices to analyze the model in this region [37].  $\square$ 

#### 3.2. Stability analysis of model's equilibria

# 3.2.1. The disease-free equilibrium and basic reproduction number of the model

The disease-free equilibrium (DFE) of the model (2.3), denoted by  $E_0^*$ , is given by

$$E_0^* = \left(S_0^*, 0, 0, 0, 0, 0, 0\right) = \left(\frac{\Lambda}{\mu}, 0, 0, 0, 0, 0\right). \tag{3.7}$$

Applying the next-gen matrix approach given in [38] to system (2.3), yields the basic reproduction number ( $R_0$ ) of the model as follows: The transfer matrices are given as:

where,  $\epsilon_1 = \theta + \mu$ ,  $\epsilon_2 = \delta + \gamma + \mu$ ,  $\epsilon_3 = \eta_1 + \mu$ . Thus,  $R_0$  of the model (2.3) is given by

$$R_0 = \rho(FV^{-1}) = \frac{\Lambda\alpha\theta\sigma\epsilon_3}{\kappa\mu\mu_b\epsilon_1\Big(\mu\epsilon_2 + \eta_1(\delta + \mu + \tau\gamma)\Big)}.$$
(3.8)

# 3.2.2. Local stability of the DFE of the model

In accordance with Theorem 2 in [38], the result of the local stability of  $E_0^*$  is provided as follows.

**Theorem 3.3.** The DFE,  $E_0^*$ , given in Eq. (3.7) is locally asymptotically stable if  $R_0 < 1$  and unstable if  $R_0 > 1$ .

Biologically, Theorem 3.3 implies that melioidosis infection will eventually diminish in the population if  $R_0 < 1$  and if the initial population sizes of the sub-classes (2.3) are within the basin of attraction of  $E_0^*$ . Hence, individuals in the infected population do not acquire additional infections.

# 3.2.3. Existence of endemic equilibrium of the model

Let an endemic equilibrium of the system (2.3) be denoted by  $E_e^* = (S^*, E^*, I^*, R_1^*, R_2^*, P^*)$ . Then the components of  $E_e^*$  satisfy the following system:

$$\begin{cases} \Lambda - (\boldsymbol{\Phi}^* + \mu)S^* = 0, \\ \boldsymbol{\Phi}^*(S^* + \eta_2 R_2^*) - \epsilon_1 E^* = 0, \\ \theta E^* + \eta_1 R_1^* - \epsilon_2 I^* = 0, \\ (1 - \tau)\gamma I^* - \epsilon_3 R_1^* = 0, \\ \tau \gamma I^* - (\mu + \eta_2 \boldsymbol{\Phi}^*)R_2^* = 0, \\ \sigma I^* - \mu_b P^* = 0, \end{cases}$$
(3.9)

where,  $\Phi^* = \frac{\alpha P^*}{r_+ P^*}$  is the force of infection at the endemic equilibrium. Solving Eq. (2.2) at the endemic equilibrium, for  $P^*$ , yields

$$P^* = \frac{\kappa \Phi^*}{\alpha - \Phi^*}.\tag{3.10}$$

At  $E_e^*$ ,  $P^* > 0$  and  $\frac{P^*}{\kappa + P^*} < 1$ , thus  $\alpha - \Phi^* = \alpha \left(1 - \frac{P^*}{\kappa + P^*}\right) > 0$ . Substituting (3.10) into the last equation of the system (3.9), gives

$$I^* = \frac{\kappa \mu_b \Phi^*}{\sigma(\alpha - \Phi^*)} > 0, \text{ for } \Phi^* > 0.$$
(3.11)

By combining Eq. (3.11) with the fourth and fifth equations of system (3.9), we obtain

$$\begin{cases}
R_1^* = \frac{\kappa \mu_b (1 - \tau) \gamma \Phi^*}{\epsilon_3 \sigma(\alpha - \Phi^*)}, \\
R_2^* = \frac{\kappa \mu_b \tau \gamma \Phi^*}{\sigma(\alpha - \Phi^*) \left(\mu + \eta_2 \Phi^*\right)}.
\end{cases} (3.12)$$

Combining Eq. (3.11), the third equation of (3.9) and the first equation of (3.12), gives

$$E^* = \frac{\kappa \mu_b \left( \mu \epsilon_2 + \eta_1 (\delta + \mu + \tau \gamma) \right) \Phi^*}{\theta \epsilon_3 \sigma (\alpha - \Phi^*)}. \tag{3.13}$$

Again, solving the first equation of (3.9) for  $S^*$ , yields

$$S^* = \frac{\Lambda}{\Phi^* + \mu}.\tag{3.14}$$

Lastly, substituting the Eqs. (3.14), (3.13) and the second equation of (3.12) into the second equation of the system (3.9), and solving for  $\Phi^*$ , we obtain a third degree equation in  $\Phi^*$ , given as follows

$$P_3(\Phi^*) = \Phi^* P_2(\Phi^*) = 0$$
, where  $P_2(\Phi^*) = A_2(\Phi^*)^2 + A_1\Phi^* + A_0$ . (3.15)

Hence,  $E_{\rho}^{*}$  of the melioidosis model (2.3) satisfy the quadratic equation in  $\Phi^{*}$  given by

$$P_2(\Phi^*) = A_2(\Phi^*)^2 + A_1\Phi^* + A_0 = 0, \tag{3.16}$$

where.

$$\begin{split} A_0 &= \kappa \mu^2 \mu_b \epsilon_1 \Big(\mu \epsilon_2 + \eta_1 (\delta + \mu + \tau \gamma) \Big) (R_0 - 1), (A_0 > 0 \text{ if } R_0 > 1, A_0 = 0 \text{ if } R_0 = 1, \text{and } A_0 < 0 \text{ if } R_0 < 1), \\ A_2 &= -\eta_2 \Big[ \Lambda \theta \sigma \epsilon_3 + \kappa \mu_b \Big( (1 - \tau) \mu \theta \gamma + (\mu \theta + \eta_1 \epsilon_1) (\mu + \delta) + \mu (\mu \eta_2 + \tau \gamma \eta_1) \Big) \Big] < 0, \quad \text{(always)} \end{split}$$

$$A_{1} = \kappa \mu \mu_{b} \epsilon_{1} \Big( \mu \epsilon_{2} + \eta_{1} (\delta + \mu + \tau \gamma) \Big) (R_{0} - 1) - \Lambda \theta \sigma \epsilon_{3} \mu + \kappa \mu \mu_{b} \Big[ \tau \gamma \theta \epsilon_{3} \eta_{2} - \epsilon_{1} \Big( \mu \epsilon_{2} + \eta_{1} (\delta + \mu + \tau \gamma) \Big) \Big]. \tag{3.17}$$

From Eq. (3.17) the expression

$$\kappa \mu \mu_b \epsilon_1 \Big( \mu \epsilon_2 + \eta_1 (\delta + \mu + \tau \gamma) \Big) (R_0 - 1) - \Lambda \theta \sigma \epsilon_3 \mu < 0, \text{ for } R_0 \le 1.$$
(3.18)

Also, 
$$\tau \gamma \theta \epsilon_3 \eta_2 - \epsilon_1 \left( \mu \epsilon_2 + \eta_1 (\delta + \mu + \tau \gamma) \right) \le \tau \gamma \theta \epsilon_3 - \epsilon_1 \left( \mu \epsilon_2 + \eta_1 (\delta + \mu + \tau \gamma) \right) (\because \tau \gamma \theta \epsilon_3 \eta_2 \le \tau \gamma \theta \epsilon_3, \text{ for } 0 \le \eta_2 \le 1).$$
But,  $\kappa \mu \mu_b \left[ \tau \gamma \theta \epsilon_3 - \epsilon_1 \left( \mu \epsilon_2 + \eta_1 (\delta + \mu + \tau \gamma) \right) \right] = -\kappa \mu \mu_b \left( (1 - \tau) \mu \theta \gamma + (\mu \theta + \eta_1 \epsilon_1) (\mu + \delta) + \mu (\mu \eta_2 + \tau \gamma \eta_1) \right) < 0.$  Thus,
$$\kappa \mu \mu_b \left[ \tau \gamma \theta \epsilon_3 \eta_2 - \epsilon_1 \left( \mu \epsilon_2 + \eta_1 (\delta + \mu + \tau \gamma) \right) \right] < 0. \tag{3.19}$$

Therefore, from the Eqs. (3.18) and (3.19), we get  $A_1 < 0$ , for  $R_0 \le 1$ .

The existence of the disease persistence equilibrium of the model (2.3) depends on the roots of the quadratic Eq. (3.16). All three coefficients of  $P_2(\Phi^*)$  are negative for  $R_0 < 1$ . Since the discriminant  $A_1^2 - 4A_0A_2 \neq 0$  for  $R_0 < 1$ , equation in (3.16) has two distinct non-zero roots, say,  $r_1$  and  $r_2$ . These roots satisfy the following conditions:  $r_1r_2 = \frac{A_0}{A_2} > 0$  and  $r_1 + r_2 = -\frac{A_1}{A_2} < 0$ . Thus, the two roots have negative signs, which are not feasible (biologically insignificant) when  $R_0 < 1$ . Moreover,  $\Phi^* = -\frac{A_1}{A_2} < 0$  is the only root of  $P_2(\Phi^*)$  at  $R_0 = 1$ . As a result, the model has no positive force of infection (feasible solution) for  $R_0 \leq 1$ . Consequently, the model system (2.3) has no positive endemic equilibrium for  $R_0 \leq 1$ . On the other hand, the coefficient  $A_0 > 0$  for  $R_0 > 1$ . In this case, the discriminant,  $A_1^2 - 4A_0A_2 > 0$ . It follows that,  $P_2(\Phi^*)$  has two different non-zero real roots for  $R_0 > 1$ , that satisfying  $r_1r_2 = \frac{A_0}{A_2} < 0$ . This indicates that  $r_1$  and  $r_2$  have opposite sings. Hence, the model has a unique positive endemic equilibrium for  $R_0 > 1$  in the presence of relapse and re-infection. Furthermore, if  $n_2 = 0$  (in the absence of relapse), the quadratic equation  $P_2(\Phi^*) = 0$  in (3.16) reduces into a linear equation  $A_1^*\Phi^* + A_0 = 0$  and it has unique solution  $\Phi^* = -\frac{A_0}{A_1^*} > 0$  if  $R_0 > 1$ , and  $\Phi^* = -\frac{A_0}{A_1^*} < 0$  if  $R_0 < 1$ , where

 $A_1^* = -\mu \Big[ \Lambda \theta \sigma \epsilon_3 + \kappa \mu_b \epsilon_1 \Big( \mu \epsilon_2 + \eta_1 (\delta + \mu + \tau \gamma) \Big) \Big] < 0$ . Therefore, model (2.3) has a unique endemic equilibrium  $E_e^*$  for  $R_0 > 1$  and lacks any positive endemic equilibrium for  $R_0 \le 1$ . This result indicates the absence of a backward bifurcation in both scenarios, with and without recurrent cases (relapse and re-infection). Unlike the model proposed in this study, other compartmental models with recurrent cases experience backward bifurcation. From an epidemiological standpoint, eliminating the disease in the population is possible when  $R_0 \le 1$ , while the disease infection will endure within the population if  $R_0 > 1$ . The results can be summarized by the following theorem.

**Theorem 3.4** (Existence of the Endemic Equilibrium). The model (2.3)

- (i) has precisely one unique endemic equilibrium in the presence and absence of recurrent when  $R_0 > 1$ ,
- (ii) has no positive endemic equilibrium (in the presence and absence of recurrent) if  $R_0 \le 1$ .

# 3.2.4. Global stability of the DFE of the model

We use the direct Lyapunov approach given in [39] to prove the global asymptotic stability of  $E_0^*$ . This necessitates a scalar function  $\Pi_0(\xi)$ ,  $\xi \in \mathbb{R}^6$ , defined on an open set  $U_0$  that includes  $E_0^*$  and satisfies the following criteria.

- (i)  $\Pi_0(E_0^*) = 0$ ,
- (ii)  $\Pi_0(\xi) > 0$ , for all  $\xi \in U_0 \setminus E_0$ , (iii)  $\frac{d\Pi_0}{dt} < 0$ , for all  $\xi \in U_0 \setminus E_0^*$  and  $\frac{d\Pi_0}{dt} = 0$  at  $E_0^*$ .

The global asymptotic stability of  $E_0^*$  is established as follows.

**Theorem 3.5.** The DFE,  $E_0^*$ , given by (3.7) is globally asymptotically stable (GAS) if  $R_0 \le 1$ .

**Proof.** If  $R_0 < 1$ , a unique locally asymptotically stable DFE exists according to Theorem 3.3. Consider the following a Lyapunov

$$\Pi_0 = \frac{\theta}{\epsilon_1} E + I + \frac{\eta_1}{\epsilon_3} R_1 + \frac{\Lambda \alpha \theta}{\kappa \mu_b \mu \eta_1} P.$$

The time derivative of  $\Pi_0$  along the model's solutions is provided as:

$$\begin{split} &\Pi_0' = \frac{\theta}{\epsilon_1} E' + I' + \frac{\eta_1}{\epsilon_3} R_1' + \frac{\Lambda \alpha \theta}{\kappa \mu_b \mu \eta_1} P' \\ &= \frac{\theta}{\epsilon_1} \Big( \varPhi(S + \eta_2 R_2) - \epsilon_1 E \Big) + \theta E + \eta_1 R_1 - \epsilon_2 I + \frac{\eta_1}{\epsilon_3} \Big( (1 - \tau) \gamma I - \epsilon_3 R_1 \Big) + \frac{\Lambda \alpha \theta}{\kappa \mu_b \mu \eta_1} \Big( \sigma I - \mu_b P \Big) \\ &= \Big( \frac{\alpha \theta P}{(\kappa + P) \epsilon_1} S - \frac{\Lambda \alpha \theta P}{\kappa \mu \eta_1} \Big) + \frac{\eta_2 \alpha \theta P}{(\kappa + P) \epsilon_1} R_2 + \frac{\Lambda \alpha \theta \sigma I}{\kappa \mu_b \mu \epsilon_1} - \frac{\Big( \mu \epsilon_2 + \eta_1 (\delta + \mu + \tau \gamma) \Big)}{\epsilon_3} I \\ &= \frac{\alpha \theta P}{\kappa \epsilon_1} \Big( \frac{\kappa}{\kappa + P} S + \frac{\eta_2 \kappa}{\kappa + P} R_2 - \frac{\Lambda}{\mu} \Big) + \frac{\Lambda \alpha \theta \sigma \epsilon_3 - \kappa \mu_b \mu \epsilon_1 \Big( \mu \epsilon_2 + \eta_1 (\delta + \mu + \tau \gamma) \Big)}{\kappa \mu_b \mu \epsilon_1 \epsilon_3} I \\ &= \frac{\alpha \theta P}{\kappa \epsilon_1} \Big( \frac{\kappa}{\kappa + P} S + \frac{\kappa}{\kappa + P} \eta_2 R_2 - \frac{\Lambda}{\mu} \Big) + \frac{\Big( \mu \epsilon_2 + \eta_1 (\delta + \mu + \tau \gamma) \Big)}{\epsilon_3} (R_0 - 1) I \\ &= \frac{\alpha \theta P}{\kappa \epsilon_1} \Big( \frac{\kappa}{\kappa + P} (S + \eta_2 R_2) - \frac{\Lambda}{\mu} \Big) + \frac{\Big( \mu \epsilon_2 + \eta_1 (\delta + \mu + \tau \gamma) \Big)}{\epsilon_3} (R_0 - 1) I, \end{split}$$

since the state variables are non-negative, and  $\kappa < \kappa + P(\text{or } \frac{\kappa}{\kappa + P} < 1), \eta_2 R_2 \le R_2$  for  $0 \le \eta_2 \le 1$ ), we obtained,  $\Pi_0'(t) < 1$ 

 $\frac{\alpha\theta P}{\kappa\epsilon_1}\Big((S+R_2)-\frac{\Lambda}{\mu}\Big)+\frac{\Big(\mu\epsilon_2+\eta_1(\delta+\mu+\tau\gamma)\Big)}{\epsilon_3}(R_0-1)I.$  Note that  $S+R_2< N\leq \frac{\Lambda}{\mu}$  in  $U_0\setminus E_0$ . As the model parameters are non-negative,  $\Pi_0'(t)<0$  in  $U_0\setminus E_0$  and provided that  $R_0\leq 1$ , and  $\Pi_0'=0$  if and only if  $E=I=R_1=P=0$  (or at  $E_0^*$ ). Thus, according to Lasalle's Invariance Principle [39],

$$(E(t), I(t), R_1(t), P(t)) \to (0, 0, 0, 0) \text{ as } t \to \infty.$$
 (3.21)

From (3.21), it follows that,  $\lim_{t\to\infty}\sup E(t)=0$ ,  $\lim_{t\to\infty}\sup I(t)=0$ ,  $\lim_{t\to\infty}\sup R_1(t)=0$  and  $\lim_{t\to\infty}\sup P(t)=0$ . Using the approach given in [40,41], for sufficient small number  $\epsilon_0$ , there exist constants  $q_1, q_2, q_3$  and  $q_4$  such that  $\lim_{t\to\infty} \sup E(t) \le \epsilon_0 \ \forall t > 0$  $q_1, \lim_{t \to \infty} \sup I(t) \le \epsilon_0 \ \forall t > q_2, \lim_{t \to \infty} \sup R_1(t) \le \epsilon_0 \ \forall t > q_3, \ \text{and} \ \lim_{t \to \infty} \sup P(t) \le \epsilon_0 \ \forall t > q_4. \ \text{Thus, from the fifth equation of the } results of the support of the$ system (2.3), for  $t > \max\{q_1, q_2, q_3, q_4\}$ , we have

 $R_2'(t) \le \tau \gamma \epsilon_0 - \mu R_2$ . As a result, by comparison theorem in [42],

$$R_2^{\infty} = \lim_{t \to \infty} \sup R_2(t) \le \frac{\tau \gamma \varepsilon_0}{\mu}.$$
 (3.22)

Letting,  $\epsilon_0 \to 0$  in (3.22), gives

$$R_2^{\infty} = \lim \sup_{t \to \infty} R_2(t) \le 0. \tag{3.23}$$

Furthermore, by using  $\lim_{t\to\infty}\inf E(t)=0$ ,  $\lim_{t\to\infty}\inf I(t)=0$ ,  $\lim_{t\to\infty}\inf R_1(t)=0$ , and  $\lim_{t\to\infty}\inf P(t)=0$ , one can verify that

$$R_{2\infty} = \lim_{t \to \infty} \inf R_2(t) \ge 0. \tag{3.24}$$

From (3.23) and (3.24) it follows that,  $R_2^{\infty} \le 0 \le R_{2\infty}$ . Therefore,  $R_2(t) \to 0$ , regardless of the initial population size  $R_2(0)$ . Likewise, it can be shown that  $S(t) \to \frac{\Lambda}{u}$  as  $t \to \infty$ .

As a result, every solution trajectory of the system (2.3), with the initial population size in  $D_1$  converges to  $E_0^*$  as  $t \to \infty$  when  $R_0 \le 1$ . Biologically this implies that the susceptible individuals do not acquire additional infections when  $R_0 \le 1$ . Therefore, in this case, the infection can be eradicated from the population over time.  $\square$ 

# 3.2.5. Global stability of the endemic equilibrium of the model

For  $R_0 > 1$ , there is a single positive endemic equilibrium,  $E_e^*$ , for the model (2.3) as stated in Theorem 3.4. The next result addresses the global asymptotic stability of  $E_e^*$  by using a suitable chosen Lyapunov function.

**Theorem 3.6.** For  $R_0 > 1$ , the endemic equilibrium,  $E_e^*$  of the model (2.3) is GAS in  $D_1 \setminus D_0$ ,  $D_0 = \{ (S, E, I, R_1, R_1, P) : E = I = R_1 = P = 0 \}$ .

**Proof.** Consider the following candidate for a Lyapunov function:  $\Pi_1(S, E, I, R_1, P) = \frac{1}{2} \Big( (S - S^*) + (E - E^*) + (I - I^*) + (R_1 - R_1^*) + (R_2 - R_2^*) \Big)^2 + \frac{1}{2} (P - P^*)^2$ , with its time derivative

$$\Pi_{1}'(t) = \left( (S + E + I + R_{1} + R_{2}) - (S^{*} + E^{*} + I^{*} + R_{1}^{*} + R_{2}^{*}) \right) \left( S'(t) + E'(t) + I'(t) + R_{1}'(t) + R_{2}'(t) \right) + (P - P^{*})(P'(t)).$$
(3.25)

Adding the first five equations of the system (3.9), we obtain

$$\frac{\Lambda}{\mu} - \frac{\delta}{\mu} I^* = S^* + E^* + I^* + R_1^* + R_2^*. \tag{3.26}$$

Also, from the last equation of the system (3.9), we have

$$P^* = \frac{\sigma}{\mu_b} I^* \le \frac{\sigma}{\mu_b} (S^* + E^* + I^* + R_1^* + R_2^*). \tag{3.27}$$

Note that  $N(t) \le \frac{\Lambda}{\mu}$  in  $D_1$ . Because the model parameters and variables of infective classes are non-negative, combining Eqs. (2.1), (2.3), (3.4) (3.25), (3.26), and (3.27), yields

$$\begin{split} H_1'(t) &= \left(N(t) - (\frac{\Lambda}{\mu} - \frac{\delta}{\mu}I^*)\right) \left(\Lambda - \mu N(t) - \delta I(t)\right) + \left(P(t) - \frac{\sigma}{\mu_b}I^*\right) \left(\sigma I - \mu_b P(t)\right) \\ &= -\left(\frac{\Lambda}{\mu} - \frac{\delta}{\mu}I^* - N(t)\right) \left(\Lambda - \mu N(t) - \delta I(t)\right) - \left(\frac{\sigma}{\mu_b}I^* - P(t)\right) \left(\sigma I - \mu_b P(t)\right) \\ &< -\left(\frac{\Lambda}{\mu} - N(t)\right) \left(\Lambda - \mu N(t)\right) - \left(\frac{\sigma}{\mu_b}(S^* + E^* + I^* + R_1^* + R_2^*) - P(t)\right) \left(\sigma I - \mu_b P(t)\right) \\ &< -\left(\frac{\Lambda}{\mu} - N(t)\right) \left(\Lambda - \mu N(t)\right) - \left(\frac{\sigma}{\mu_b}(\frac{\Lambda}{\mu} - \frac{\delta}{\mu}I^*) - P(t)\right) \left(\sigma I - \mu_b P(t)\right) \\ &< -\mu\left(\frac{\Lambda}{\mu} - N(t)\right) \left(\frac{\Lambda}{\mu} - N(t)\right) - \mu_b\left(\frac{\sigma}{\mu_b}\frac{\Lambda}{\mu} - P(t)\right) \left(\frac{\sigma}{\mu_b}I - P(t)\right) \\ &< -\mu\left(\frac{\Lambda}{\mu} - N(t)\right) \left(\frac{\Lambda}{\mu} - N(t)\right) - \left(\frac{\Lambda\sigma}{\mu\mu_b} - P(t)\right) \left(\frac{\Lambda\sigma}{\mu\mu_b} - P(t)\right) \quad (\because I < \frac{\Lambda}{\mu} \quad \text{in} \quad D_1) \\ &< -\left[\mu\left(\frac{\Lambda}{\mu} - N(t)\right)^2 + \mu_b\left(\frac{\Lambda\sigma}{\mu\mu_b} - P(t)\right)^2\right] < 0. \end{split}$$

Thus,  $\Pi_1'(t) < 0$  in  $D_1 \setminus D_0$  when  $R_0 > 1$ . Since  $\Pi_1$  is a well-defined candidate for the Lyapunov function in  $D_1$  and according to Lasalle's Invariance Principle [39], we conclude that  $E_e^*$  is GAS when  $R_0 > 1$ . This result indicates that every trajectory of the model (2.3) solutions with initial population sizes in  $D_1 \setminus D_0$ , eventually moves towards the respective unique endemic equilibrium,  $E_e^*$ , of the model  $t \to \infty$  for  $R_0 > 1$ . In biological terms, the melioidosis infection will endure within the population.

# 4. Sensitivity analysis

In this section, we perform sensitivity analysis using a normalized forward sensitivity index to identify parameters with high influence on  $R_0$ . This assists in suggesting appropriate control strategies for mitigating the spread of the disease. We utilize the approach given in [43,44]. The forward sensitivity index of  $R_0$  with respect to a particular parameter  $\varphi$  is provided by

$$Y_{\varphi}^{R_0} = \frac{\partial R_0}{\partial \varphi} \times \frac{\varphi}{R_0}. \tag{4.1}$$

By using Eq. (4.1), the sensitivity index of parameters of  $R_0$  is computed and presented in Table 2, ranking from the most influential parameter to the least. The parameter values from Table 1 are used.

Based on the Table 2 and Fig. 2, the parameters  $\alpha$ ,  $\sigma$ ,  $\Lambda$ ,  $\theta$  and  $\eta_1$  have positive sensitivity index values, indicating a direct influence of the parameters on the magnitude of  $R_0$ . In contrast,  $\mu_b$ ,  $\kappa$ ,  $\mu_b$ ,  $\kappa$ ,  $\mu_b$ ,  $\kappa$ ,  $\mu_b$ ,  $\kappa$ ,  $\mu_b$ ,  $\kappa$ , and the parameters on  $R_0$ . Also, we observed that  $\alpha$ ,  $\sigma$ ,  $\mu_b$ ,  $\kappa$  are the most influencing parameters on  $R_0$  (directly or indirectly), as confirmed in Fig. 2 and Table 2. For example, reducing the value of  $\alpha$  or  $\sigma$  by  $\zeta$ % would also reduce the value of  $R_0$  by the same percentage  $\zeta$ %.

**Table 2** Sensitivity indices for parameters of  $R_0$ 

Parameter	Value	Sensitivity index	
α	0.0185	1.0000	
$\sigma$	0.13	1.0000	
$\mu_b$	0.02	-1.0000	
κ	5000	-1.0000	
Λ	$\mu \times N_0$	1.0000	
μ	1 65×365	-1.0077	
δ	0.005	-0.8325	
γ	0.0037	-0.1605	
$\theta$	$\frac{1}{9}$	0.0004	
$\eta_1$	0.069	0.0003	

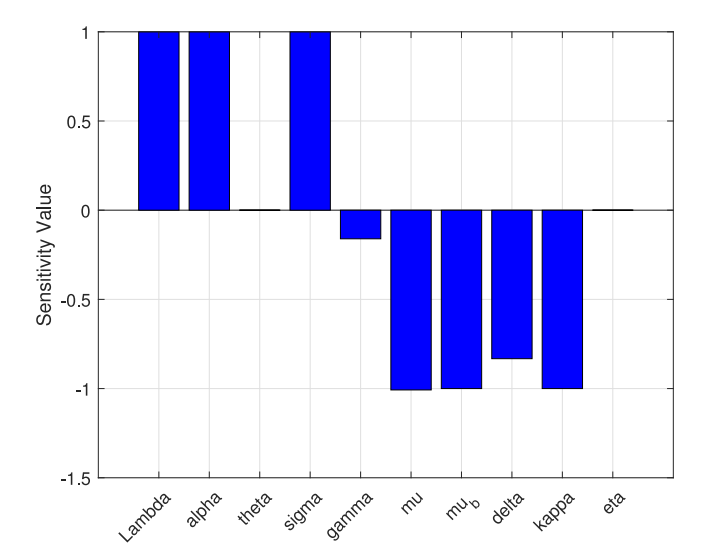


Fig. 2. Plot shows sensitivity indices for each parameter of  $R_0$ .

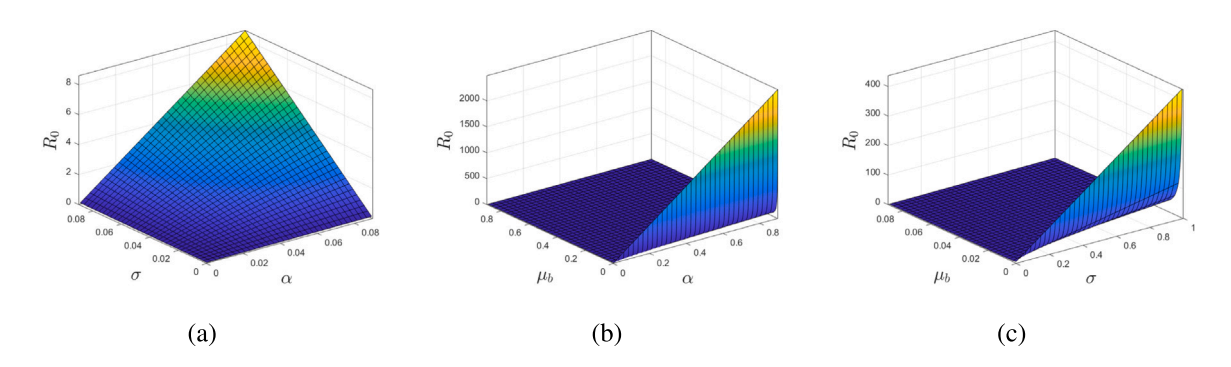


Fig. 3. Graphical results showing the impact of the most influencing parameters on  $R_0$ ; (a)  $R_0$  vs  $\alpha$  and  $\sigma$ , (b)  $R_0$  vs  $\alpha$  and  $\mu_b$ , and (c)  $R_0$  vs  $\sigma$  and  $\mu_b$ . The parameter values given in Table 1 are used.

On the contrary, increasing the value of  $\mu_b$  or  $\kappa$  by 15% would decrease  $R_0$  by 13.04632%. Furthermore, the numerical illustration of the changing effects of parameters  $\alpha$ ,  $\sigma$  and  $\mu_b$  on  $R_0$  can be seen in surface and contour plots refer, Figs. 3 and 4. From Figs. 3(a) – 3(b) and Figs. 4(a) – 4(b), it is evident that increasing the value of  $\alpha$ , will lead to the endemic condition. A similar observation can be made for the varying impact of  $\alpha$  from the plots. On the other hand,  $R_0$  decreases as the pathogen's mortality rate increases, as depicted in Figs. 3(b) – 3(c) and Figs. 4(b) – 4(c). In view of the results of sensitivity analysis, control strategies for  $\alpha$  and  $\sigma$  will sufficiently reduce the spread of melioidosis. Moreover, a strategy that increases the mortality rate of B. pseudomallei, will be effective in controlling environment-born melioidosis with recurrent. Consequently, the control efforts could be employed through prevention measures and treatment for classes of I and  $R_1$  to mitigate the disease spread within the population for this specific study.

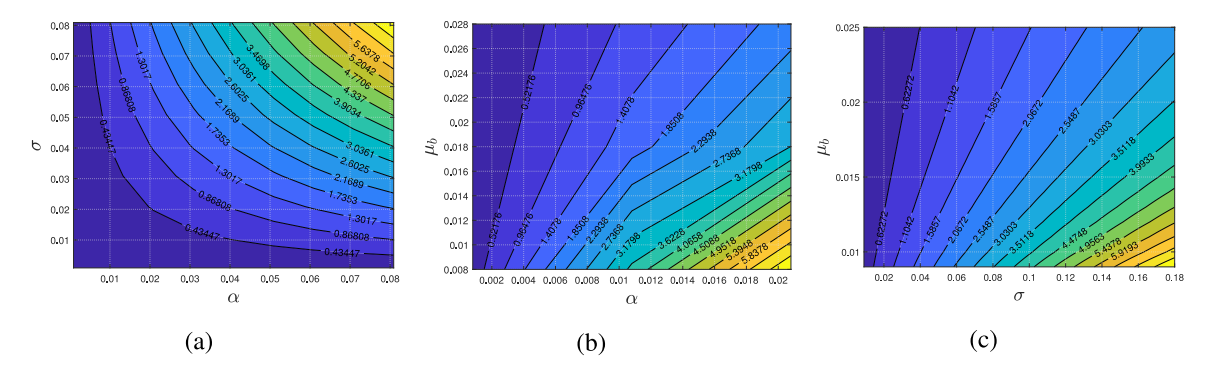


Fig. 4. Graphical results showing contour plots of  $R_0$  in (a)  $\alpha\sigma$  plane, (b)  $\alpha\mu_b$  plane, and (c)  $\sigma\mu_b$  plane.

#### 5. Numerical stability analysis of the equilibria of the model

In this section, we present numerical results for the global dynamics of the autonomous model (2.3) to support the qualitative analysis of the model. We use the ode45 algorithm in MATLAB to accomplish this. The model parameters used for simulations are provided in Table 1, and the initial population sizes are set as:

$$M_0^* = (S(0), E(0), I(0), (0), R_1(0), R_2(0), P(0)) = (450, 50, 20, 10, 5, 200).$$

$$(5.1)$$

So, using the explicit formula in (3.8), the basic reproduction number is found as  $R_0 \approx 2.1416$ . Using Eqs. (3.10)–(3.14) and (3.16) the unique positive disease presence equilibrium of the model is obtained as,

 $E_e^*=(248.9221,0.1092,2.0195,0.0801,44.3091,13.1266)$  for the unique positive value,  $\Phi\approx4.844118684001455\times10^{-5}$ . In this instance, each model solution trajectory moves towards the equilibrium point  $E_e^*$  over time, as shown in Figs. 6(a)-6(d). This result suggests that all infected classes persist in the population. In epidemiological terms, this means that the melioidosis infection will persist in the population for  $R_0>1$ . Moreover, the model has the unique positive,  $E_e^*=(250.4653,0.1079,1.9961,0.0792,45.5589,12.9749)$  for  $\Phi\approx4.7883\times10^{-5}$  in the absence of relapse. However, setting the values of the most sensitive parameters as  $(\alpha,\sigma,\mu_b,\kappa)=(0.008,0.09,0.01,7000)$  yields  $R_0\approx0.9159<1$ . As a result, the model has the unique DFE,  $E_0^*=(\frac{\Lambda}{\mu},0,0,0,0,0)$ , which is globally asymptotically stable. Therefore, all model solution trajectories move to  $E_0^*$  eventually, regardless of the initial population sizes as shown in Figs. 5(a)-5(d). From a biological perspective, this suggests that the disease will die out from the population over time. To eliminate the melioidosis infection disease, it is essential to minimize the value of  $R_0$  as much as possible by implementing appropriate intervention strategies. The impact of various control interventions on reducing disease spread is discussed in the optimal control model section.

# 5.1. Impact of $\eta_1$ and $\eta_2$ on I(t), $R_1(t)$ and $R_2(t)$

The impact of the parameters relapse rate  $\eta_1$  and reinfection rate  $\eta_2$  on the dynamics of infectious and recovered ( $R_1$  and  $R_2$ ) human populations are illustrated in Figs. 7 and 8. Fig. 7(a) shows that the class of pseudo-recovered humans,  $R_1(t)$ , decreases over time as  $\eta_1$  increases. Meanwhile, the population of infectious humans rises as  $\eta_1$  increases, as depicted in Fig. 7(b). Likewise, it can be seen in Figs. 8(a) and 8(b) that  $R_2(t)$  decreases as  $\eta_2$  rises in value, consequently leading to an increase in the number of infectious humans. Therefore, these results suggest that appropriate preventive measures for classes of  $R_1(t)$  and  $R_2(t)$  should be implemented to minimize disease recurrence, ultimately leading to a reduction in the infectious human population.

# 6. Analysis of optimal control model

In this section, an optimal control model for the dynamics of melioidosis with recurrence is formulated by incorporating the time-dependent control functions. Based on the sensitivity analysis results, the following control measures are considered to determine effective and cost-effective strategies for eradicating environment-borne melioidosis:  $\omega_1(t)$ , denotes prevention efforts like wearing protective footwear and gloves, treating unsafe drinking water, and raising public awareness through information and education [2,45];  $\omega_2(t)$ , represents treatment efforts to prevent relapse using eradicating antibiotics (e.g., TMP–SMX for 140 days, TMP–SMX plus doxycycline for over 84 days, or TMP–SMX plus doxycycline plus chloramphenicol for more than 84 days [24]);  $\omega_3(t)$ , denotes treatment control for I using antibiotics such as ceftazidime, carbapenem, or cefepime. Thus, the model (2.3) with

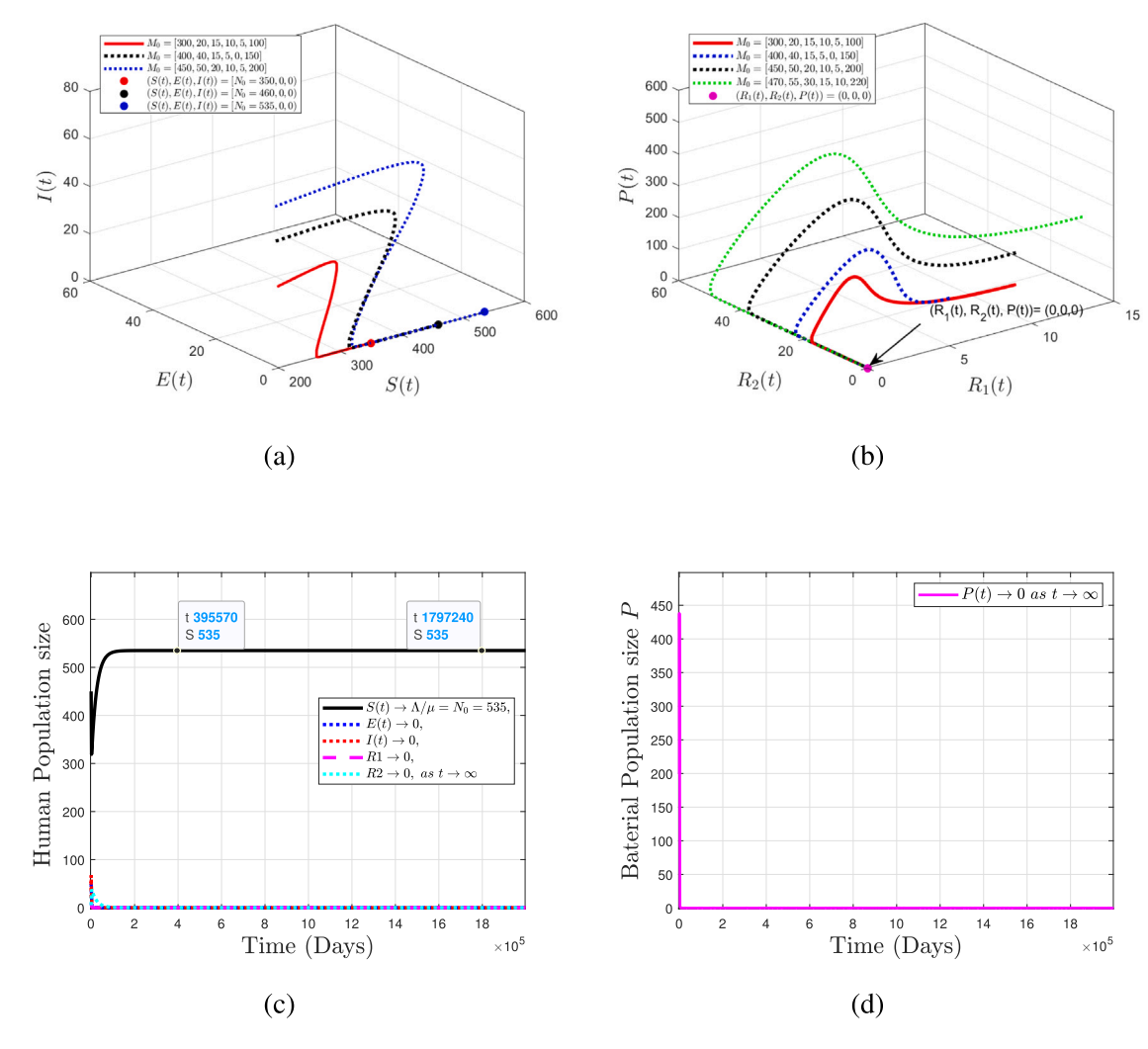


Fig. 5. Graphical results showing the convergence of solutions of the model (2.3) over time with different initial values to the components of  $E_0^*$ ; convergence of (a) (S, E, I) to  $(\frac{A}{\mu}, 0, 0)$  in 3-D, (b)  $(R_1, R_2, P)$  to (0, 0, 0) in 3-D, (c)  $S, E, I, R_1$ , and  $R_2$  to  $\frac{A}{\mu}, 0, 0, 0$ , and 0, respectively, in 2-D, (d) P to 0 in 2-D. The parameter values given in Table 1 are used except  $\alpha = 0.008$ ,  $\sigma = 0.09$ ,  $\mu_b = 0.01$ , and  $\kappa = 7000$  (so that,  $R_0 \approx 0.9159 < 1$ ).

the presence of these controls is formulated as follows.

$$\begin{cases} S'(t) = \Lambda - ((1 - \omega_1)\Phi + \mu)S, \\ E'(t) = (1 - \omega_1)\Phi(S + \eta_2 R_2) - (\theta + \mu)E, \\ I'(t) = \theta E + (1 - \omega_2)\eta_1 R_1 - (\gamma + \delta + \varrho \omega_3 + \mu)I, \\ R'_1(t) = (1 - \tau)(\gamma + \varrho \omega_3)I - \left((1 - \omega_2)\eta_1 + \mu\right)R_1, \\ R'_2(t) = \tau(\gamma + \varrho \omega_3)I - \left(\mu + (1 - \omega_1)\eta_2 \Phi\right)R_2, \\ P'(t) = (1 - \omega_1)\sigma I - \mu_b P, \end{cases}$$

$$(6.1)$$

subject to the initial conditions:  $S(0) \ge 0$ ,  $E(0) \ge 0$ , where, the coefficient e(0) is the treatment control rate in infectious class. This problem aims to minimize the infectious human population while keeping the costs of implementing controls as small as possible. Thus, the objective functional subject to the state system (6.1) is given by

$$O(\omega_1, \omega_2, \omega_3) = \int_0^{T_f} \left( W_0 I + \frac{1}{2} \sum_{n=1}^3 W_n \omega_n^2 \right) dt, \tag{6.2}$$

where,  $T_f$  is the final time, the coefficient  $W_0$  declares the positive weight constant of I, while  $W_1, W_2$  and  $W_3$  are relative cost positive weights for optimal controls  $\omega_1, \omega_2$  and  $\omega_3$ , respectively. We quantify the cost of each control by considering a quadratic

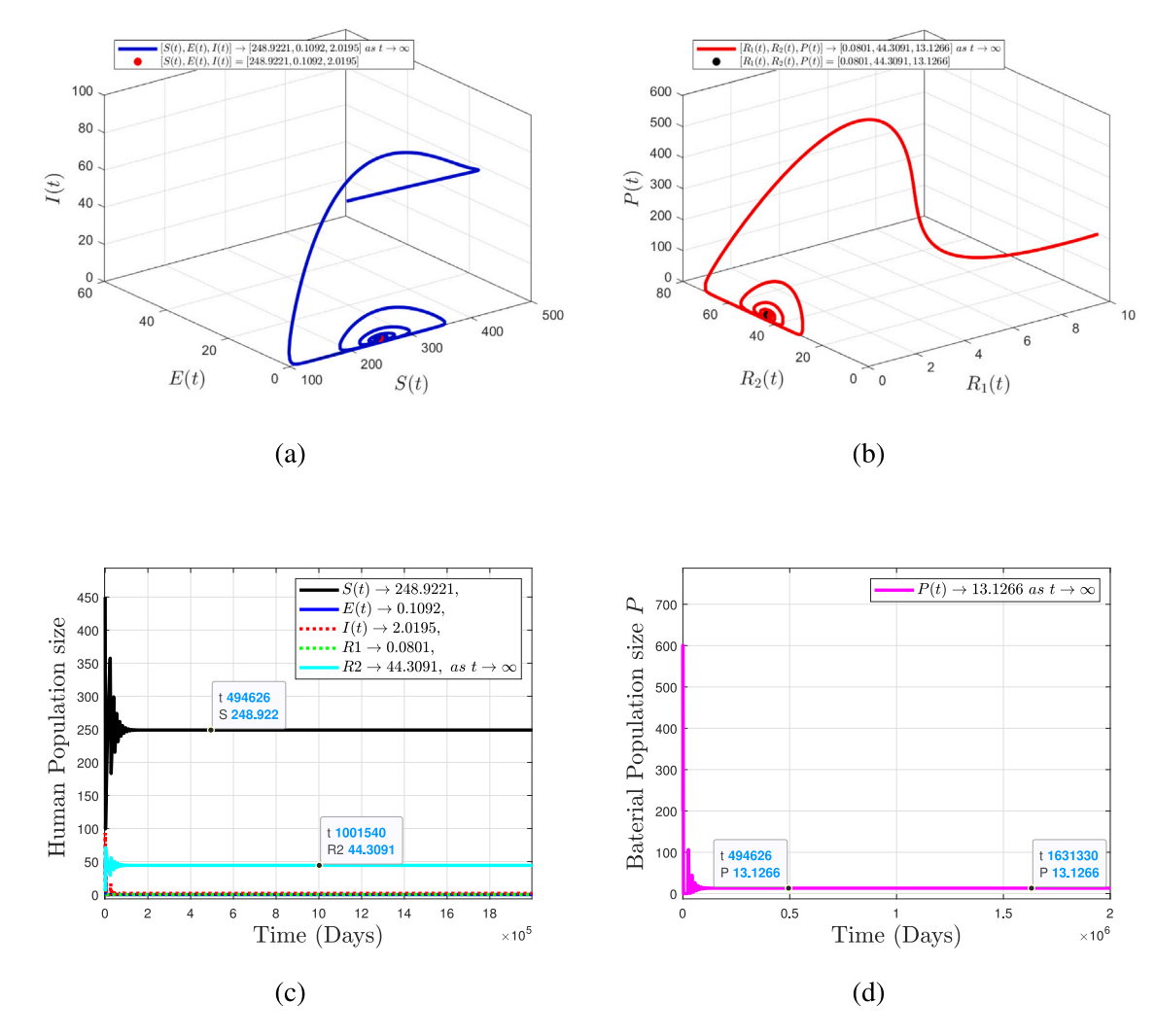


Fig. 6. Graphical results showing the convergence of solutions of the model (2.3) over time with different initial values to the components of  $E_e^*$ ; convergence of (a) (S, E, I) to (248.9221, 0.1092, 2.0195) in 3-D, (b)  $(R_1, R_2, P)$  to (0.0801, 44.3091, 13.1266) in 3-D, (c)  $S, E, I, R_1$ , and  $R_2$  to 248.9221, 0.1092, 2.0195, 0.0801, and 44.3091, respectively, in 2-D, (d) P to 13.1266 in 2-D. The parameter values given in Table 1 are used (so that,  $R_0 \approx 2.1416 > 1$ ).

objective function. This is because there is no linear relationship between the intervention's impact and cost for infective classes. The quadratic nature of the control cost is consistent with previous literature [46–48]. The goal is to find an optimal control,  $\omega^* = (\omega_1^*, \omega_2^*, \omega_3^*)$ , satisfying

$$O(\omega_1^*, \omega_1^*, \omega_2^*) = \inf\{O(\omega_1, \omega_2, \omega_3) : \omega_1, \omega_2, \omega_3 \in \Omega\},\tag{6.3}$$

where,  $\Omega = \{(\omega_1(t), \omega_2(t), \omega_3(t)) : 0 \le \omega_n(t) \le 1, t \in [0, T_f]\}$  is a non-empty control set and each  $\omega_n(t)$  is Lebesgue measurable, n = 1, 2, 3.

A Hamiltonian H, of the optimal control problem, based on PMP [49] is formulated as follows:

$$H = W_0 I + \frac{1}{2} \sum_{n=1}^{3} W_n \omega_n^2 + J_1 S'(t) + J_2 E'(t) + J_3 I'(t) + J_4 R'_1(t) + J_5 R'_2(t) + J_6 P'(t).$$
(6.4)

where,  $J_n$  (n = 1, 2, ..., 6) are the co-state variables corresponding to the state variables.

# 6.1. Existence of an optimal control

We now establish and prove a result for the existence of the optimal control,  $\omega^*$ , that satisfy Eq. (6.3).

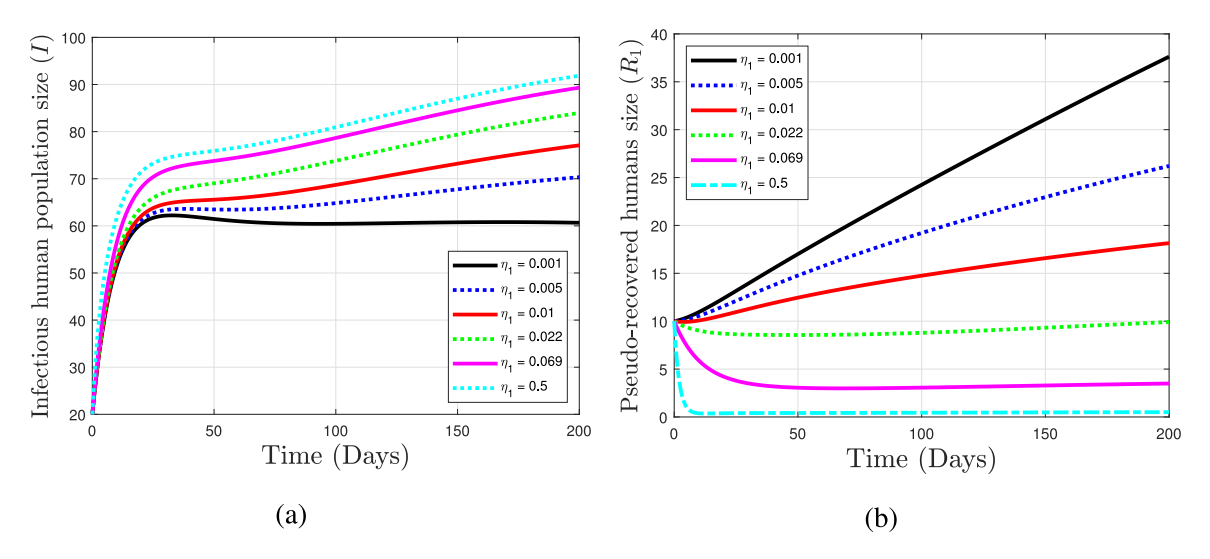


Fig. 7. Plots demonstrating the impact of  $\eta_1$  on the populations of (a) infected humans and (b) recovered individuals with relapse  $(R_1)$ .

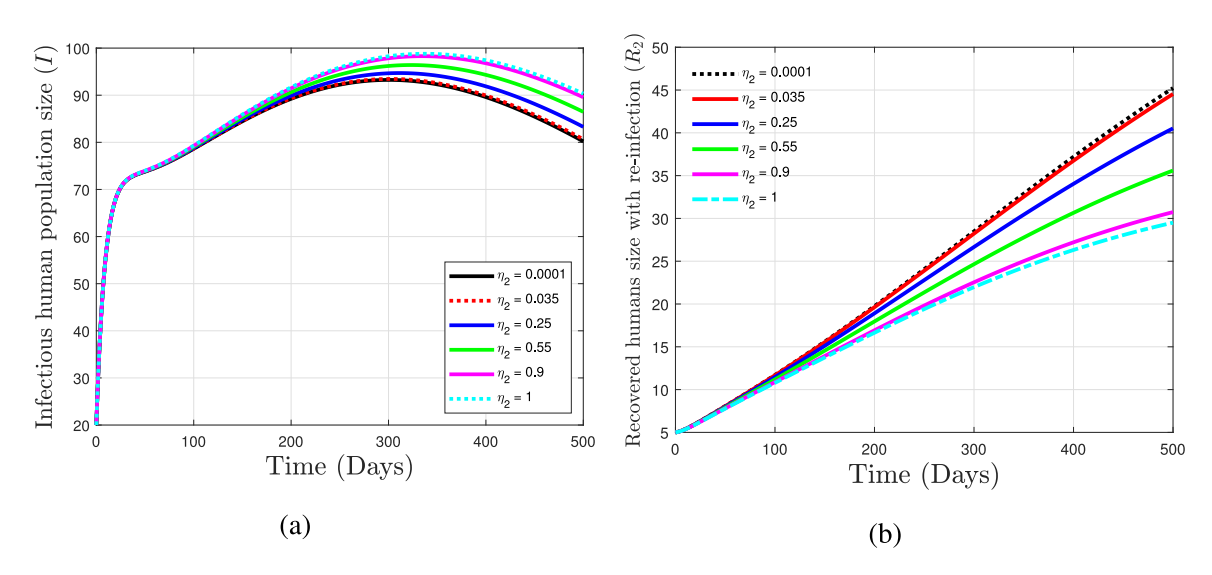


Fig. 8. Plots illustrating the effects of the re-infection rate,  $\eta_2$ , on the populations of (a) infected humans and (b) recovered individuals with re-infection ( $R_2$ ).

**Theorem 6.1.** Suppose the objective function O is defined on the control set  $\Omega$  subject to the system (6.1) with non-negative initial population sizes at t = 0, then there exists an optimal control  $\omega^* = (\omega_1^*, \omega_2^*, \omega_3^*)$  such that  $O(\omega^*) = \inf\{O(\omega_1, \omega_2, \omega_3) : \omega_1, \omega_2, \omega_3 \in \Omega\}$ , if the following conditions given in [50] hold:

- (i) The admissible control set is closed and convex,
- (ii) The state system (6.1) is bounded by a linear function in the state and control variables,
- (iii) The Lagrangian of the optimal control in (6.2) is convex with respect to the controls,
- (iv) There exist constants  $k_1, k_2 > 0$  and  $k_3 > 1$  such that the Lagrangian  $\ell$  is bounded below by

$$k_1 \left( \sum_{n=1}^3 |\omega_n| \right)^{\frac{k_3}{2}} - k_2.$$

**Proof.** (i) Let  $\Omega_0 = \{(\omega_1, \omega_2, \omega_3) : 0 \le \omega_n \le 1, n = 1, 2, 3\}$  be the control set. Then,  $\Omega_0$ , is closed and convex by definition.

(ii) Let  $Q = (S, E, I, R_1, R_2, P)$  be the state variables of the optimal system (6.1) and  $\Psi(Q, \omega)$  be the right-hand side of the system (6.1), where,  $\omega = (\omega_1, \omega_2, \omega_3)^T$ . Following, the same approach given in [51,52], the system (6.1) can be written as

 $\Psi(Q,\omega) = \Psi_1(Q) + \Psi_2(Q)\omega$ , where

$$\Psi_{1}(Q) = \begin{bmatrix}
\Lambda - (\Phi + \mu)S \\
\Phi(S + \eta_{2}R_{2}) - (\theta + \mu)E \\
\theta E + \eta_{1}R_{1} - (\gamma + \delta + \mu)I \\
(1 - \tau)\gamma I - (\eta_{1} + \mu)R_{1} \\
\tau\gamma I - (\mu + \eta_{2}\Phi)R_{2}
\end{bmatrix}, \quad
\Psi_{2}(Q) = \begin{bmatrix}
\Phi S & 0 & 0 \\
-\Phi(S + \eta_{2}R_{2}) & 0 & 0 \\
0 & -\eta_{1}R_{1} & -\varrho I \\
0 & \eta_{1}R_{1} & (1 - \tau)\varrho I
\end{bmatrix}.$$

$$\Phi\eta_{2}R_{2} & 0 & \tau\varrho I \\
-\Phi\eta_{2}R_{2} & 0 & \tau\varrho I \\
-\sigma I & 0 & 0
\end{bmatrix}.$$
(6.5)

Thus, we obtain  $\|\Psi(Q)\| \le \|\Psi_1(Q)\| + \|\Psi_2(Q)\| \|\omega\| \le \max\{\Gamma_0, \Gamma_1\}(1 + \|\omega\|)$ , where,

$$\Gamma_0 = \frac{\Lambda}{\mu} \sqrt{\Delta_0}$$
, and  $\Gamma_1 = \frac{\Lambda}{\mu} \sqrt{\Delta_1}$ , (6.6)

with,

$$\Delta_0 = 2\alpha^2 + 2\eta_1^2 + 3\eta_2^2 + \sigma^2 + \varrho^2(1 + \tau^2 + (1 - \tau)^2), \text{ and } \Delta_1 = \mu^2 + \alpha^2(1 + 3\eta_2^2) + (\theta + \eta_2)^2 + \sigma^2 + \gamma^2(\tau^2 + (1 - \tau)^2).$$

(iii) The Lagrangian of the optimal control is given by

$$\ell(I,\omega) = W_0 I + \ell_1(\omega), \tag{6.7}$$

where,  $\ell_1(\omega) = \frac{1}{2} \sum_{n=1}^3 W_n \omega_n^2$ . We need to show that the function  $\ell_1(\omega)$  is convex on the control  $\omega$ . To perform this, define the function  $\varphi: \Omega_0 \to \mathbb{R}$  by  $\varphi(\omega) = \frac{1}{2}\omega^2$ . Let  $y, z \in \Omega_0$ , with  $y = (y_1, y_2, y_3)$  and  $z = (z_1, z_2, z_3)$  and  $\zeta \in [0, 1]$ . Then, using the idea of convex set in [53], we need to show

$$\varphi(\zeta y + (1 - \zeta)z) \le \zeta \varphi(y) + (1 - \zeta)\varphi(z), \ \forall \zeta \in [0, 1].$$

Since  $\zeta^2 \le \zeta$ ,  $\forall \zeta \in [0, 1]$ , we obtained

$$\varphi(\zeta y + (1 - \zeta)z) - (\zeta \varphi(y) + (1 - \zeta)\varphi(z)) = \frac{1}{2}(\zeta y + (1 - \zeta)z)^{2} - \frac{1}{2}(\zeta y^{2} + (1 - \zeta)z^{2})$$

$$= \frac{1}{2}(\zeta^{2} - \zeta)(y - z)^{2} \le 0.$$
(6.8)

As a result, the function  $\ell_1(\omega)$  is convex on  $\omega$ .

(iv) The Lagrangian in Eq. (6.7) is the sum of non-negative terms  $W_0I$  and  $\ell_1(\omega)$ , the last condition is shown as follow:

$$\ell(I,\omega) = W_0 I + \frac{1}{2} \sum_{n=1}^{3} W_n \omega_n^2 \ge \frac{1}{2} \sum_{n=1}^{4} W_n \omega_n^2 \ge \frac{k_1}{2} \left( \sum_{n=1}^{3} |\omega_n|^2 \right)^{\frac{k_3}{2}} - k_2, \tag{6.9}$$

where,  $k_1 = \min\{W_1, W_2, W_3\}, k_2 > 0 \text{ and } k_3 = 2.$ 

**Theorem 6.2.** Suppose the set  $\omega^* = (\omega_1^*, \omega_2^*, \omega_3^*)$  minimizes O over  $\Omega$  subject to the optimal system (6.1), then there exist adjoint variables  $J_1, J_2, J_3, J_4, J_5, J_6$  that satisfying

$$\begin{split} \frac{dJ_{1}}{dt} &= (J_{1} - J_{2})(1 - \omega_{1})\boldsymbol{\Phi} + J_{1}\mu, \\ \frac{dJ_{2}}{dt} &= (J_{2} - J_{3})\boldsymbol{\theta} + J_{2}\mu, \\ \frac{dJ_{3}}{dt} &= -W_{0} + J_{3}(\gamma + \delta + \rho\omega_{3} + \mu) - J_{4}(\gamma + \rho\omega_{3})(1 - \tau) - J_{5}(\gamma + \rho\omega_{3})\tau - J_{6}\sigma(1 - \omega_{1}), \\ \frac{dJ_{4}}{dt} &= (J_{4} - J_{3})(1 - \omega_{2})\eta_{1} + J_{4}\mu, \\ \frac{dJ_{5}}{dt} &= (J_{5} - J_{2})(1 - \omega_{1})\eta_{2}\boldsymbol{\Phi} + J_{5}\mu, \\ \frac{dJ_{6}}{dt} &= (J_{1} - J_{2})(1 - \omega_{1})\frac{\alpha\kappa S}{(\kappa + P)^{2}} + (J_{5} - J_{2})(1 - \omega_{1})\frac{\alpha\kappa\eta_{2}R_{2}}{(\kappa + P)^{2}} + \mu_{b}J_{6}, \end{split}$$

$$(6.10)$$

and with final time conditions.

$$J_n(T_f) = 0, n = 1, 2, \dots, 6.$$
 (6.11)

Furthermore, the optimal controls  $\omega_k^*$ , k = 1, 2, 3 that minimizes O over  $\Omega$  are given by

$$\begin{split} \omega_{1}^{*} &= \max \bigg\{ 0, \min \bigg\{ \frac{(J_{2} - J_{1}) \varPhi S + (J_{2} - J_{5}) \varPhi \eta_{2} R_{2} + \sigma I J_{6}}{W_{1}}, 1 \bigg\} \bigg\}, \quad \omega_{2}^{*} &= \max \bigg\{ 0, \min \bigg\{ \frac{(J_{3} - J_{4}) \eta_{1} R_{1}}{W_{2}}, 1 \bigg\} \bigg\}, \\ \omega_{3}^{*} &= \max \bigg\{ 0, \min \bigg\{ \frac{(J_{3} - J_{4}(1 - \tau) - J_{5}\tau) \varrho I}{W_{3}}, 1 \bigg\} \bigg\}. \end{split} \tag{6.12}$$

**Proof.** Let  $\chi^* = (S^*, E^*, I^*, R_1^*, R_2^*, P^*)$  and  $\omega^* = (\omega_1^*, \omega_2^*, \omega_3^*)$  be corresponding solutions satisfying (6.1) and (6.3), respectively. We use the standard results presented in [54] to derive the adjoint system and the optimal control. With the help of PMP [54], the adjoint system is determined by taking the negative of the derivative of H (6.4) with respect to associated state variables  $S, E, I, R_1, R_2, P$  respectively:

$$-\frac{dJ_1}{dt} = \frac{\partial H}{\partial S}, \quad -\frac{dJ_2}{dt} = \frac{\partial H}{\partial E}, \quad -\frac{dJ_3}{dt} = \frac{\partial H}{\partial I}, \quad -\frac{dJ_4}{dt} = \frac{\partial H}{\partial R_1}, \quad -\frac{dJ_5}{dt} = \frac{\partial H}{\partial R_2}, \quad -\frac{dJ_6}{dt} = \frac{\partial H}{\partial P}, \tag{6.13}$$

with  $J_n(T) = 0, n = 1, 2, ..., 6$ . Lastly, to find optimal controls in the interior of the control set  $\Omega$ , we employ

$$\frac{\partial H}{\partial \omega_k} = 0, \text{ for } \omega_k^*, \quad k = 1, 2, 3.$$
(6.14)

Solving Eq. (6.14) for each optimal control  $\omega_1^*$ ,  $\omega_2^*$  and  $\omega_2^*$  gives the relation which is the same as given in (6.12).  $\square$ 

#### 6.2. Numerical simulations

This section presents numerical simulations of the optimality system, comprising the state system (6.1), co-state system (6.10) with its final conditions (6.11) and the characterization of the optimal controls (6.12) for the melioidosis model. To demonstrate this, we use the forward-backward sweep method in MATLAB [55]. We set the tolerance to  $\pi=0.0001$ , to reduce the error. The aim is to illustrate the most effective and cost-effective control strategies for mitigating the spread of the disease. The parameter values used in the simulations are listed in Table 1, while the initial population sizes for each class are given in Eq. (5.1). Moreover, the weight constant of the infectious class is  $W_0=10$  and weight constant values for the controls are assumed as;  $w_1=10, w_2=10, w_3=20$ . The treatment control rate is  $\varrho=0.75$ . The choice of the treatment control rate is based on the relapse rates of melioidosis infection, ranging from 13% to 23% in patients [22,56].

The numerical experiments of the optimality system are performed to assess the effectiveness of seven different optimal control strategies, which are grouped into three scenarios as follows:

Scenario I: Optimal use of single control:

- Strategy A: impact of prevention control  $(\omega_1 \neq 0, \omega_2 = \omega_3 = 0)$ ,
- Strategy *B*: impact of relapse preventive effort  $R_1$  ( $\omega_2 \neq 0, \omega_1 = \omega_3 = 0$ ),
- Strategy C: impact of treatment control of  $R_2$  ( $\omega_3 \neq 0, \omega_2 = \omega_1 = 0$ ).

Scenario II: Optimal use of double controls:

- Strategy D: Combination of optimal controls  $\omega_1$  and  $\omega_2$ ,
- Strategy E: Combination of optimal controls  $\omega_1$  and  $\omega_3$ ,
- Strategy F: Combination of optimal controls  $\omega_2$  and  $\omega_3$ .

Scenario III: Optimal use of all controls:

• Strategy G: Combination of the optimal controls,  $\omega_1, \omega_2$ , and  $\omega_3$ .

#### 6.2.1. Scenario I: Optimal use of single control

This scenario compares the effectiveness of the optimal strategies A, B and C on classes of I and P. The numerical results of this scenario are depicted in Fig. 9 and Table 3. Fig. 9(a) and Table 3 illustrate that strategy C has the highest number of infectious averted followed by strategy A, then strategy B. Similarly, Fig. 9(b), shows that strategy C is the most effective to eliminate the pathogen population in the environment compared to strategies A and B. Furthermore, the optimal control profiles for the three strategies are given in Figs. 10 (a) – 10(c). The control profile for strategy A shows that the prevention effort  $\omega_1$  should be maintained at the upper bound (100%) for the first 135.5 days and then reduced to zero (lower bound) for the rest of the simulation period, as depicted in Fig. 10(a). The control profile of strategy B in Fig. 10(a) illustrates that the optimal control  $\omega_2$  is consistently at the upper bound throughout the entire intervention period (for 200 days). The control profile for strategy C is revealed in Fig. 10(c), where it is observed that the control was at maximum effort for 82.6 days before reducing to the lower bound.

# 6.2.2. Scenario II: Optimal use of double controls

In this scenario, we implement the optimal strategies D, E and F to compare their effectiveness. The simulation results of this scenario are shown in Fig. 11. As depicted in Figs. 11(a) and 11(b) the number of infectious individuals and the size of the bacterial population decrease more rapidly when implementing strategies D, E and F compare to the case without strategies. However, strategy F leads to a greater decrease in the size of I compared to strategies D and E, as confirmed in Fig. 11(a) and Table 3. A similar result is evident in Fig. 11(b) for the bacterial class. Furthermore, the optimal control profiles in these strategies are given in Figs. 12(a) - 12(c). The control profile of strategy D in Fig. 12(a) shows that the preventive measure  $\omega_1$  should be maintained at the maximum effort for the first 134 days and subsequently it should be gradually reduced to lower bound for the rest of the simulation time, while the control  $\omega_2$  is maintained at 100% throughout the entire intervention period. Likewise, the control profile of strategy F in Fig. 12(c) shows that the control  $\omega_2$  should be maintained at the maximum effort for the first 15 days and subsequently it should be gradually reduced to lower bound for the rest of the simulation time, while the control  $\omega_3$  is maintained at 100% throughout the entire intervention period. The control profile of strategy E in Fig. 12(b) reveals that the controls  $\omega_1$  and  $\omega_3$  maintain the upper bound for the first 27 and 66 days, respectively before lowering gradually to zero rapidly in the rest of simulation period.

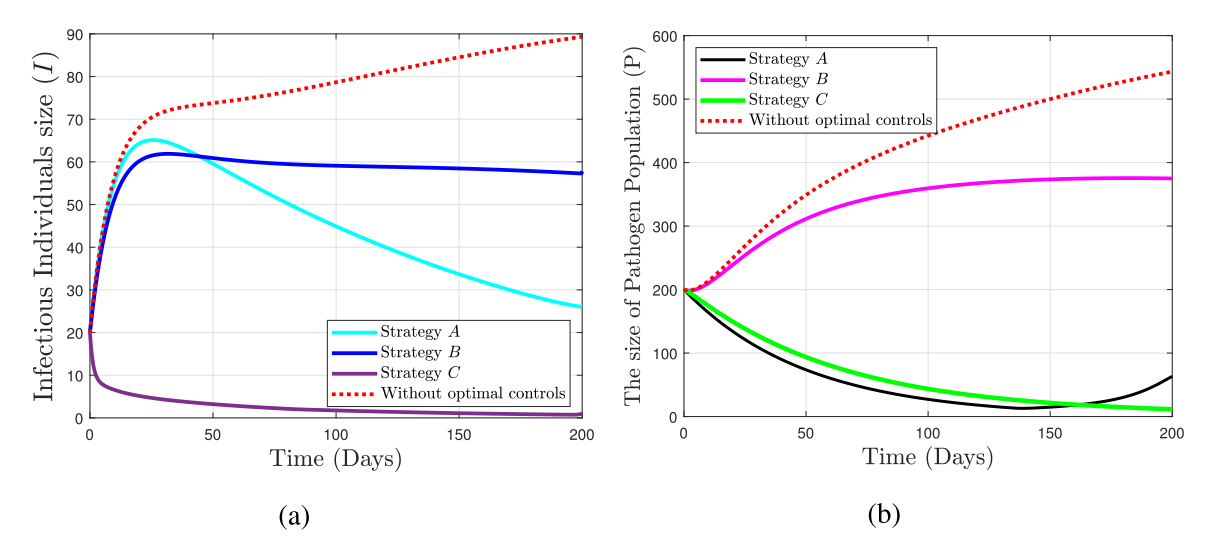


Fig. 9. Plots showing the dynamics of the model with and without Strategy A, B & and C on classes of (a) I(t) and (b) P(t).

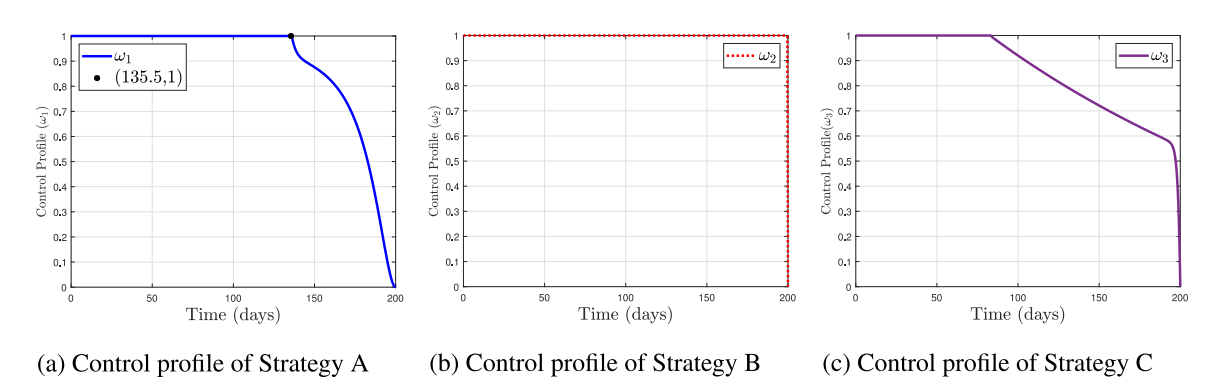


Fig. 10. Plots showing the control profiles of the strategies A, B & and C.

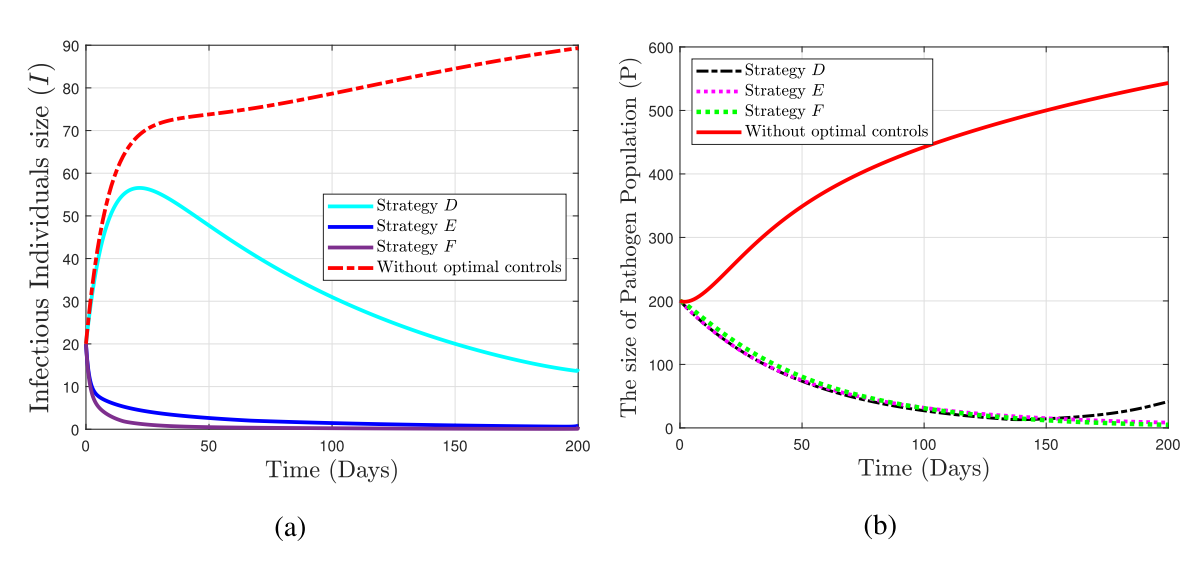


Fig. 11. Plots showing the dynamics of the model with and without Strategies D, E & and F on classes of (a) I(t) and (b) P(t).

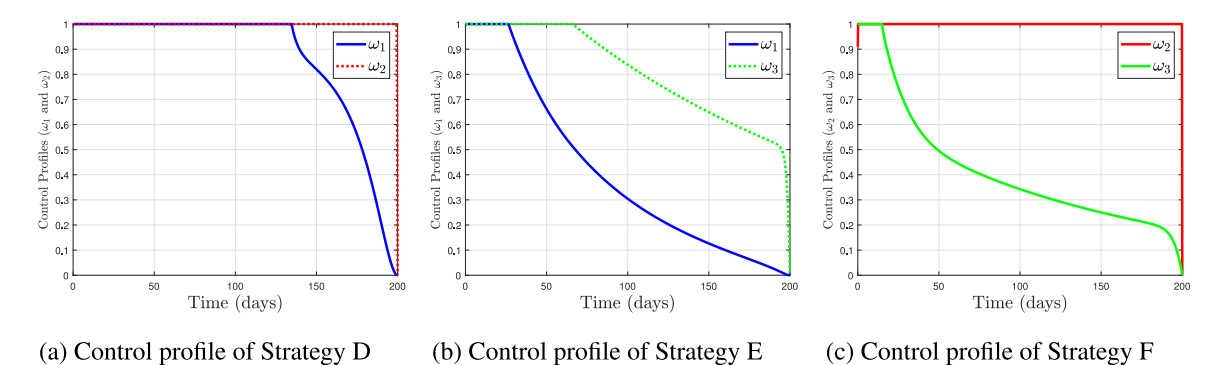


Fig. 12. Plots showing the control profiles of the three strategies D, E & and F.

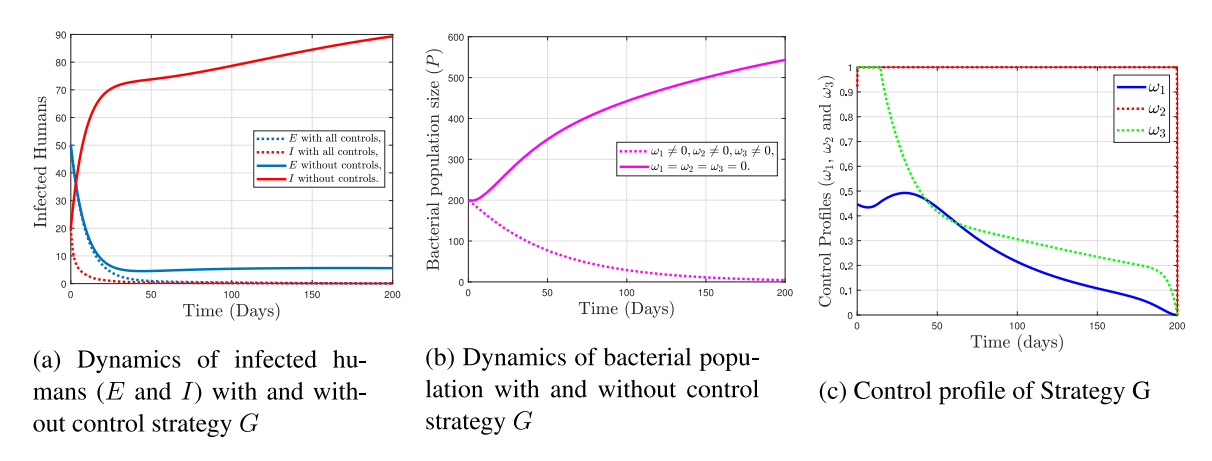


Fig. 13. Plots showing the impact of Strategy G on classes of infected humans and pathogens.

# 6.2.3. Scenario III: Optimal use of all optimal controls

In this scenario, we implement all the control functions  $\omega_1, \omega_2$  and  $\omega_3$ . The graphical results of this scenario are illustrated in Fig. 13. Figs. 13(a) and 13(b) indicate that the number of infected humans (E and I) and the pathogen population decrease significantly when strategy G is used, while the populations of infectious humans (I) and pathogens increase in the absence of this strategy throughout simulation time. The control profiles of the last scenario are depicted in Fig. 13(c). In Fig. 13(c), it can be seen that control  $\omega_3$  are kept at 100% for 13.2 days before gradually declining to zero by the end. While control  $\omega_1$  rises from 44.5% to 50% before gradually decreasing to zero at the end of the simulation period. Meanwhile, the control  $\omega_2$  is consistently at maximum effort 100% throughout the entire intervention period, as revealed in Fig. 13(c).

# 6.2.4. Comparison of the most effective strategies

Based on the results illustrated under scenarios I-III, we compare the effectiveness of strategies C, F and G to determine the most effective among them in mitigating the spread of melioidosis with recurrence. The graphical comparison results are presented in Fig. 14. As depicted in Fig. 14(a), the number of susceptible individuals in the population decreases more rapidly in the absence of strategies C, F and G than the number of susceptible individuals in the presence of the strategies throughout the simulation period. However, strategy G minimizes the number of susceptible individuals getting infected by melioidosis more effectively than strategies B and C, as observed in Fig. 14(a). Likewise, from Fig. 14(b), Fig. 15 and Table 3, we noticed that strategy G has the highest number of infected averted individuals, followed by strategy F and then strategy G. The findings from Fig. 14(G) also indicate a similar outcome for the bacterial class. Arising from the numerical results in Figs. 14(G) - (G), we conclude that strategy G is the most prominent in reducing environmental-borne melioidosis in the population, regardless of the control costs. Thus, public health centers and policymakers should prioritize implementing a strategy that combines three control measures G0 and G1 to diminish the impact of melioidosis in the community.

# 6.3. Cost-effectiveness analysis

This section presents a cost-effectiveness analysis to identify the most cost-effective strategy among optimal strategies implemented in the previous section. To perform this, we employ two approaches; the average cost-effectiveness ratio (ACER) and the incremental cost-effectiveness ratio (ICER) in the sense of [34,41,57,58].

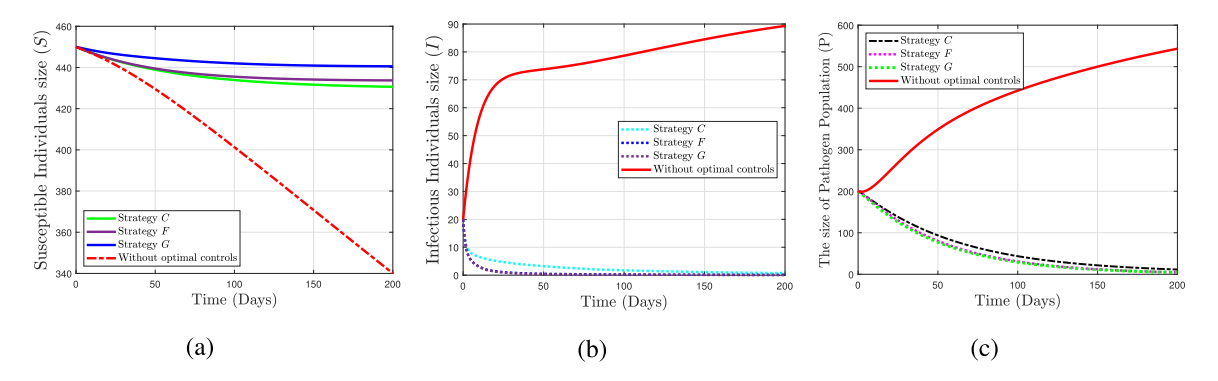


Fig. 14. Plots demonstrating the impact of the most effective strategies C, F & G on dynamic behavior of (a) susceptible individuals, (b) infectious individuals, and (c) the disease's pathogen.

Table 3
Increasing order of infection averted, Total cost and ACER.

Strategy	Infection averted	Total cost (\$)	ACER
В	19124	4996.6	0.2613
A	32 551	4192.9	0.1288
D	44 570	9048.6	0.2030
C	74751.3	7603.3	0.1017
E	75 074.7	8307.7	0.1107
F	76 549.6391	7317	0.0956
G	76 611.7	7463.8	0.0974

The ACER quantifies one strategy to its baseline option. This ratio for a particular strategy  $\phi$  is calculated as:

ACER(
$$\phi$$
) =  $\frac{\text{Total cost incurred by }\phi}{\text{Total number of infection averted by strategy }\phi}$ . (6.15)

where, numerator of (6.15) is estimated from

$$C_{\phi} = \frac{1}{2} \int_{0}^{200} \left( \sum_{n=1}^{3} W_n \omega_n^2 \right) dt$$
, and (6.16)

the total number of infections averted is calculated by subtracting the number of infectious humans with control from the number of infectious humans without control. Therefore, the total number of infections averted ( $I_{total}$ ) during the intervention period is estimated as follows:

$$I_{total} = \int_{0}^{200} I(t) dt - \int_{0}^{200} I^{*}(t) dt, \tag{6.17}$$

with,  $\int_0^{200} I(t) \, dt$  represents the total number of infectious cases without control over [0,200], and  $\int_0^{200} I^*(t) \, dt$  denotes the total number of infectious humans with control. The total cost for each of the strategies A-G is obtained using Eq. (6.16) and is given in the third column of Table 3 and in percentage by pie chart in Fig. 16. While  $I_{total}$  for the strategies is computed using Eq. (6.17) and is listed in the second column of Table 3 in increasing order of  $I_{total}$ . The ACER for optimal strategies is computed using Eq. (6.15) and presented in the 4th column of Table 3. Based on this approach, the strategy with the lowest ACER value is considered the most cost-effective. Therefore, the ACER values in Table 3 and Fig. 17 indicate that strategy F, with the smallest ACER value, is the most cost-effective strategy. This result is further supported by calculating the ICER values for the control strategies.

The second method, ICER, involves comparing the incremental difference in costs and health outcomes between two alternative intervention strategies that are competing for the same resources. The ICER value for two strategies  $S_1$  and  $S_2$  is calculated as follows:

ICER = 
$$\frac{\text{Change in total intervention costs in strategies } S_1 \text{ and } S_2}{\text{Change in the total number of infections averted in strategies } S_1 \text{ and } S_2}$$
. (6.18)

The implemented strategies are ranked according to their increasing order of  $I_{total}$  as shown in the second columns of Table 3. Based on the ICER approach, the strategy to be removed from the list of alternative strategies at each step corresponds to the largest ICER value.

We use Eq. (6.18) to calculate the ICER for strategies B and A and compare the values as follows:

$$ICER(B) = \frac{4996.6 - 0}{19124 - 0} = 0.2613, \quad ICER(A) = \frac{4192.9 - 4996.6}{32551 - 19124} = -0.0599. \tag{6.19}$$

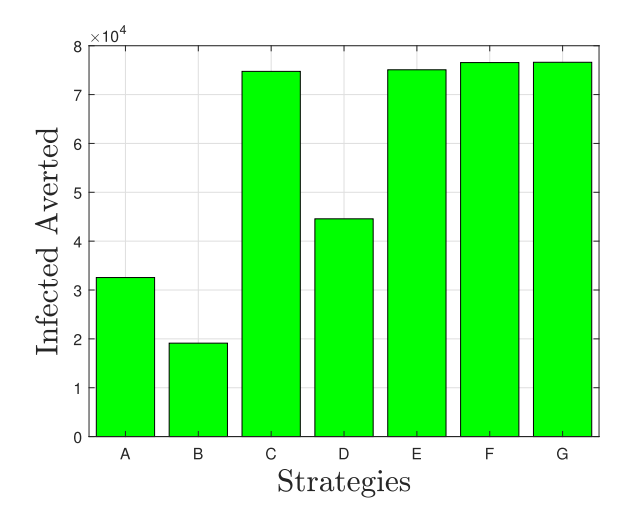


Fig. 15. Total number of infections averted for control strategies.

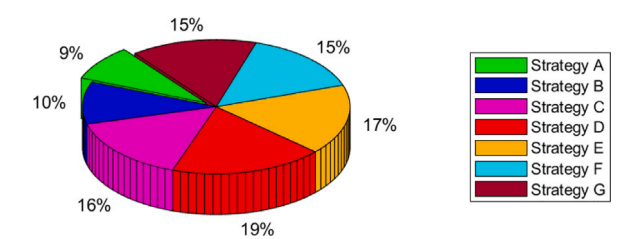


Fig. 16. Total cost produced by control strategies.

In (6.19)ICER(A) is less than ICER(B), indicating that strategy B strongly dominated by strategy A. Thus, strategy A is less expensive and more effective than strategy B. As a result, strategies A and D are compared instead of strategy B, which is excluded from the roster of intervention strategies.

$$ICER(A) = \frac{4192.9 - 0}{32551 - 0} = 0.1288, \quad ICER(D) = \frac{9048.6 - 4192.9}{44570 - 32551} = 0.4040. \tag{6.20}$$

Comparing ICER values in (6.20), the result indicates that strategy D is more costly than strategy A as ICER(D) > ICER(A). Thus, strategy D is removed from the list of alternative interventions. Hence, strategies A and C are compared.

$$ICER(A) = \frac{4192.9 - 0}{32551 - 0} = 0.1288, \quad ICER(C) = \frac{7603.3 - 4192.9}{74751.3 - 32551} = 0.0808. \tag{6.21}$$

The comparison in (6.21) shows that ICER(A) > ICER(C), as a result, strategy C is less expensive than strategy A and should be eliminated from the list of alternative interventions. We compare strategies C and E.

$$ICER(C) = \frac{7603.3 - 0}{74751.3 - 0} = 0.1017, \quad ICER(E) = \frac{8307.7 - 7603.3}{75074.7 - 74751.3} = 2.1781.$$
 (6.22)

From Eq. (6.22), it can be seen that ICER(E) > ICER(C), shows that strategy C dominates strategy E. Thus, strategy E is more expensive than strategy C. Consequently, strategy E is excluded from the list of alternative interventions. We compare strategies E & E as follow:

$$ICER(C) = \frac{7603.3 - 0}{74751.3 - 0} = 0.1017, \quad ICER(F) = \frac{7317 - 7603.3}{76549.6391 - 74751.3} = -0.1600. \tag{6.23}$$

It is evident from (6.23) that strategy C is more costly than strategy F. Consequently, strategies F & G are compared as follow:

$$ICER(F) = \frac{7317 - 0}{76549.6397 - 0} = 0.0956, \quad ICER(G) = \frac{7463.8 - 7317}{76611.7 - 76549.6397} = 2.3654.$$
 (6.24)

Finally, the values of ICER in (6.24) indicate that strategy F is less costly than strategy G. Consequently, strategy G is removed from the list of alternative interventions. Hence, strategy F (combination of optimal controls  $\omega_2$  and  $\omega_3$ ) is the most cost-effective among all implemented strategies. This outcome agrees with the results of ACER given in Table 3. This suggests that melioidosis infection with recurrent can be eliminated with minimal intervention costs by providing treatment control for the infectious class and implementing efforts to prevent the disease relapse.

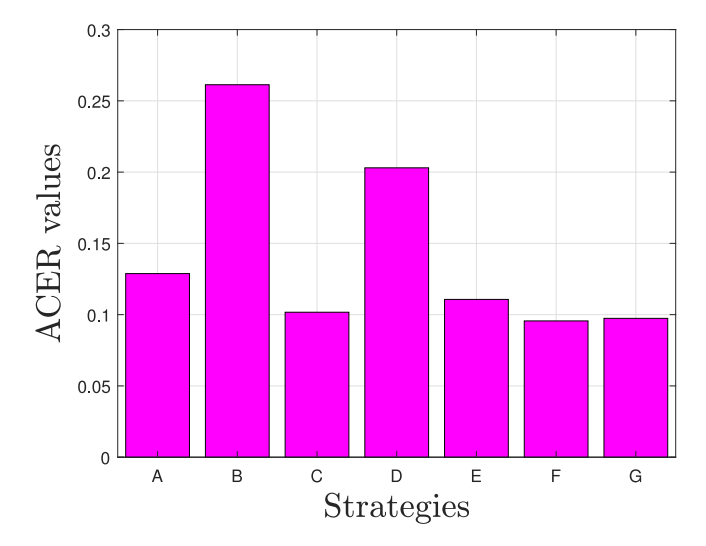


Fig. 17. ACER of control strategies.

#### 7. Conclusion

In this paper, a compartmental model of environmental-born human melioidosis dynamics with recurrent phenomena has been proposed and rigorously analyzed. The analysis of the formulated model has been performed in two parts: global stability and sensitivity analysis of the autonomous melioidosis model, and optimal control problem analysis of the model with time-dependent control functions. The basic reproduction number  $(R_0)$  of the model was obtained based on the method of the next-generation matrix. The proposed model has two unique equilibria: one is disease-free (DFE) and the other is disease-presence equilibrium  $(E_e^*)$ . Global asymptotic stability of the model's equilibria were examined using appropriate Lyapunov functions. It is shown that DFE is globally asymptotically stable when  $R_0 \le 1$ , regardless of the presence or absence of disease recurrence. Whereas, the unique endemic equilibrium is globally asymptotically stable if  $R_0$  exceeds unity, again in both the presence and absence of relapse and re-infection. Thus, the system (2.3) does not exhibit backward bifurcation phenomena with or without recurrence. This suggests that melioidosis infection can be eradicated in the population when  $R_0$  is less than one. Moreover, numerical results for the global stability of equilibria were carried out to reinforce the analytical analysis of the autonomous model using the ode45 algorithm in MATLAB. It is observed that the model solutions converge to DFE (or  $E_e^*$ ) when the basic reproduction number is less than (or greater than) one, respectively, as depicted in Figs. 5 and 6.

Next, we have formulated an optimal control problem by including three control functions: prevention effort  $\omega_1(t)$ , treatment control  $\omega_2(t)$  for the infectious class, and relapse-preventing measures using eradicating antibiotics  $\omega_3(t)$ . Pontryagin's maximum principle has been employed to obtain the necessary conditions for the optimal control problem. Numerical experiments on the non-autonomous model are conducted in three scenarios (I-III) to evaluate the effectiveness of seven different control strategies (A-G). From simulation results, we noticed that implementing all controls  $\omega_1, \omega_2$  and  $\omega_3$  simultaneously is the most effective strategy in reducing the transmission of melioidosis in the population, as shown in Figs. 10–15 and in Table 3. Meanwhile, the quantitative results from cost-effectiveness analysis indicated that implementing the combination of two controls  $\omega_2$  and  $\omega_3$  is the most cost-effective optimal strategy to minimize the disease spread with recurrent in the community, as confirmed by ICER values in Eqs. (6.19)–(6.24), and ACER values in Table 3 and in Fig. 17.

In this paper, disease transmission between humans and animals for the formulated model has not been taken into account. Although the effect of animals on disease transmission is uncommon, the impact of transmission between humans and animals on infection rates can be considered. Also, the seasonal factor's effects have not been taken into account. A more general model can be proposed, incorporating the impact of seasonal factors on melioidosis to provide more insight into the disease's transmission.

# Declaration of competing interest

The authors declare that they have no known competing financial interests or personal relationships that could have appeared to influence the work reported in this paper.

# Data availability

Data included in article/supplementary material/referenced in the article.

# References

- [1] Suntornsut Pornpan, Teparrukkul Prapit, Wongsuvan Gumphol, Chaowagul Wipada, Michie Susan, Day Nicholas PJ, et al. Effectiveness of a multifaceted prevention programme for melioidosis in diabetics (PREMEL): A stepped-wedge cluster-randomised controlled trial. PLoS Negl Trop Dis 2021;15(6):e0009060.
- [2] Mohapatra Prasanta R, Mishra Baijayantimala. Burden of melioidosis in India and south Asia: Challenges and ways forward. Lancet Reg Health-Southeast Asia 2022.
- [3] Lafontaine Eric R, Chen Zhenhai, Huertas-Diaz Maria Cristina, Dyke Jeremy S, Jelesijevic Tomislav P, Michel Frank, et al. The autotransporter protein BatA is a protective antigen against lethal aerosol infection with Burkholderia mallei and Burkholderia pseudomallei. Vaccine: X 2019;1:100002.
- [4] Anunnatsiri Siriluck, Chaowagul Wipada, Teparrukkul Prapit, Chetchotisakd Ploenchan, Tanwisaid Kittisak, Khemla Supphachoke, et al. A comparison between 12 versus 20 weeks of trimethoprim-sulfamethoxazole as oral eradication treatment for melioidosis: an open-label, pragmatic, multicenter, non-inferiority, randomized controlled trial. Clin Infect Dis 2021;73(11):e3627–33.
- [5] Limmathurotsakul Direk, Golding Nick, Dance David AB, Messina Jane P, Pigott David M, Moyes Catherine L, et al. Predicted global distribution of burkholderia pseudomallei and burden of melioidosis. Nature Microbiol 2016;1(1):1–5.
- [6] Mukhopadhyay Chiranjay, Shaw Tushar, Varghese George M, Dance David AB. Melioidosis in south Asia (India, nepal, Pakistan, bhutan and afghanistan). Trop Med Infect Dis 2018;3(2):51.
- [7] Owen William, Smith Simon, Kuruvath Sarin, Anderson David, Hanson Josh. Melioidosis of the central nervous system; A potentially lethal impersonator. IDCases 2021;23:e01015.
- [8] Mabayoje Diana Ayoola, Kenna Dervla TD, Dance David AB, NicFhogartaigh Caoimhe. Melioidosis manifesting as chronic femoral osteomyelitis in patient from Ghana. Emerg Infect Diseases 2022;28(1):201.
- [9] Chantratita Narisara, Phunpang Rungnapa, Yarasai Atchara, Dulsuk Adul, Yimthin Thatcha, Onofrey Lauren A, et al. Characteristics and one year outcomes of melioidosis patients in northeastern thailand: A prospective, multicenter cohort study. Lancet Reg Health-Southeast Asia 2023;9.
- [10] Karunanayake Panduka. Melioidosis: Clinical aspects. Clin Med 2022;22(1):6.
- [11] Aziz Ammar, Currie Bart J, Mayo Mark, Sarovich Derek S, Price Erin P. Comparative genomics confirms a rare melioidosis human-to-human transmission event and reveals incorrect phylogenomic reconstruction due to polyclonality. Microbial Genomics 2020;6(2).
- [12] Karunarathna AKTM, Mendis SA, Perera WPDP, Patabendige Geethika, Pallewatte AS, Kulatunga Aruna. A case report of melioidosis complicated by infective sacroiliitis in Sri Lanka. Trop Dis Travel Med Vaccines 2018;4(1):1–6.
- [13] Chakravorty Arindam, Heath Christopher H. Melioidosis: an updated review. Aust J General Pract 2019;48(5):327-32.
- [14] Keragala Keragala Arachchige Reshani Kaumada, Gunathilaka Maththe Gama Ralalage Shobha Sanjeewani, Senevirathna Rathnabahu Mudiyanselage Indika Sanjeewa Kumara, Jayaweera Jayaweera Arachchige Asela Sampath. Efficacy and safety of co-trimoxazole in eradication phase of melioidosis; systematic review. Ann Clin Microbiol Antimicrob 2023;22(1):74.
- [15] Halim Isra, Shaw Tushar, Tellapragada Chaitanya, Vandana KE, Mukhopadhyay Chiranjay. Melioidosis: Reinfection going incognito as relapse. Indian J Med Microbiol 2017;35(4):593-6.
- [16] Sullivan RP, Ward L, Currie BJ. Oral eradication therapy for melioidosis: important but not without risks. Int J Infect Dis 2019;80:111-4.
- [17] Sullivan Richard P, Marshall Catherine S, Anstey Nicholas M, Ward Linda, Currie Bart J. 2020 Review and revision of the 2015 Darwin melioidosis treatment guideline; paradigm drift not shift. PLoS Negl Trop Dis 2020;14(9):e0008659.
- [18] Lim Yue-Min, Vadivelu Jamuna, Mariappan Vanitha, Venkatraman Gopinath, Vellasamy Kumutha Malar. Effective therapeutic options for melioidosis: Antibiotics versus phage therapy. Pathogens 2022;12(1):11.
- [19] Fisher Dale A, Harris Patrick NA. Melioidosis: refining management of a tropical time bomb. Lancet 2014;383(9919):762-4.
- [20] Dance David. Treatment and prophylaxis of melioidosis. Int J Antimicrob Agents 2014;43(4):310-8.
- [21] Chowdhury Sukanta, Barai Lovely, Afroze Samira Rahat, Ghosh Probir Kumar, Afroz Farhana, Rahman Habibur, et al. The epidemiology of melioidosis and its association with diabetes mellitus: a systematic review and meta-analysis. Pathogens 2022;11(2):149.
- [22] Ross Brittany N, Myers Julia N, Muruato Laura A, Tapia Daniel, Torres Alfredo G. Evaluating new compounds to treat burkholderia pseudomallei infections. Front Cell Infect Microbiol 2018:8:210.
- [23] Fen Shirley Hii Yi, Tandhavanant Sarunporn, Phunpang Rungnapa, Ekchariyawat Peeraya, Saiprom Natnaree, Chewapreecha Claire, et al. Antibiotic susceptibility of clinical burkholderia pseudomallei isolates in northeast thailand during 2015–2018 and the genomic characterization of β-lactam-resistant isolates. Antimicrob Agents Chemother 2021.
- [24] Anothaisintawee Thunyarat, Harncharoenkul Krit, Poramathikul Kamonporn, Phontham Kittijarankon, Boonyarangka Parat, Kuntawunginn Worachet, et al. Efficacy of drug treatment for severe melioidosis and eradication treatment of melioidosis: A systematic review and network meta-analysis. PLoS Negl Trop Dis 2023;17(6):e0011382.
- [25] Ketheesan Natkunam. Melioidosis: a century of observation and research. Elsevier; 2012.
- [26] Chaowagul Wipada, Chierakul Wirongrong, Simpson Andrew J, Short Jennifer M, Stepniewska Kasia, Maharjan Bina, et al. Open-label randomized trial of oral trimethoprim-sulfamethoxazole, doxycycline, and chloramphenicol compared with trimethoprim-sulfamethoxazole and doxycycline for maintenance therapy of melioidosis. Antimicrob Agents Chemother 2005;49(10):4020–5.
- [27] Baba Isa Abdullahi, Rihan Fathalla A, Hincal Evren. A fractional order model that studies terrorism and corruption codynamics as epidemic disease. Chaos Solitons Fractals 2023;169:113292.
- [28] Sharomi Oluwaseun, Malik Tufail. Optimal control in epidemiology. Ann Oper Res 2017;251(1-2):55-71.
- [29] Das Dhiraj Kumar, Khajanchi Subhas, Kar TK. Transmission dynamics of tuberculosis with multiple re-infections. Chaos Solitons Fractals 2020;130:109450.
- [30] Baba Isa Abdullahi, Humphries Usa Wannasingha, Rihan Fathalla A. A well-posed fractional order cholera model with saturated incidence rate. Entropy 2023;25(2):360.
- [31] Terefe Yibeltal Adane, Kassa Semu Mitiku. Analysis of a mathematical model for the transmission dynamics of human melioidosis. Int J Biomath 2020;13(07):2050062.
- [32] Engida Habtamu Ayalew, Theuri David Mwangi, Gathungu Duncan, Gachohi John, Alemneh Haileyesus Tessema. A mathematical model analysis of the human melioidosis transmission dynamics with an asymptomatic case. Heliyon 2022;e11720.
- [33] Tavaen Sunisa, Viriyapong Ratchada. Global stability and optimal control of melioidosis transmission model with hygiene care and treatment. Int J Sci 2019;16(2):31–48.
- [34] Engida Habtamu Ayalew, Gathungu Duncan Kioi, Ferede Melkamu Molla, Belay Malede Atnaw, Kawe Patiene Chouop, Mataru Bilali. Optimal control and cost-effectiveness analysis for the human melioidosis model. Heliyon 2024;e26487.
- [35] Mahikul Wiriya, White Lisa J, Poovorawan Kittiyod, Soonthornworasiri Ngamphol, Sukontamarn Pataporn, Chanthavilay Phetsavanh, et al. Modelling population dynamics and seasonal movement to assess and predict the burden of melioidosis. PLoS Negl Trop Dis 2019;13(5):e0007380.
- [36] Lakshmikantham Vangipuram, Leela Srinivasa, Martynyuk Anatoly A. Stability analysis of nonlinear systems. Springer; 1989.
- [37] Hethcote Herbert W. The mathematics of infectious diseases. SIAM Rev 2000;42(4):599-653.
- [38] Van den Driessche Pauline, Watmough James. Reproduction numbers and sub-threshold endemic equilibria for compartmental models of disease transmission. Math Biosci 2002;180(1–2):29–48.

- [39] La Salle Joseph P. The stability of dynamical systems. SIAM; 1976.
- [40] Safi Mohammad A, Gumel Abba B. Dynamics of a model with quarantine-adjusted incidence and quarantine of susceptible individuals. J Math Anal Appl 2013;399(2):565–75.
- [41] Ghosh Mini, Olaniyi Samson, Obabiyi Olawale S. Mathematical analysis of reinfection and relapse in malaria dynamics. Appl Math Comput 2020;373:125044.
- [42] Smith HL. P. Waltman. The theory of the Chemostat. Cambridge University Press: 1995.
- [43] Chitnis Nakul, Hyman James M, Cushing Jim M. Determining important parameters in the spread of malaria through the sensitivity analysis of a mathematical model. Bull Math Biol 2008;70(5):1272.
- [44] Aldila Dipo, Angelina Michellyn. Optimal control problem and backward bifurcation on malaria transmission with vector bias. Heliyon 2021;7(4):e06824.
- [45] Benoit Tina J, Blaney David D, Gee Jay E, Elrod Mindy G, Hoffmaster Alex R, Doker Thomas J, et al. Melioidosis cases and selected reports of occupational exposures to *Burkholderia pseudomallei*—United States, 2008–2013. Morb Mortal Wkly Rep Surveill Summ 2015;64(5):1–9.
- [46] Omame Andrew, Abbas Mujahid. Modeling SARS-CoV-2 and HBV co-dynamics with optimal control. Phys A 2023;615:128607.
- [47] Liu Lili, Wang Xi, Liu Ou, Li Yazhi, Jin Zhen, Tang Sanyi, et al. Valuation and comparison of the actual and optimal control strategy in an emerging infectious disease: Implication from a COVID-19 transmission model. Infect Dis Model 2024.
- [48] Tchoumi SY, Diagne ML, Rwezaura H, Tchuenche JM. Malaria and COVID-19 co-dynamics: A mathematical model and optimal control. Appl Math Model 2021;99:294–327.
- [49] Pontryagin LS, Boltyanskii VG, Gamkrelidze RV, Mishchenko EF. The maximum principle. In: The mathematical theory of optimal processes. New York: John Wiley and Sons; 1962.
- [50] Fleming Wendell H, Rishel Raymond W. Deterministic and stochastic optimal control. Springer-Verlag; 1975.
- [51] Omame Andrew, Abbas Mujahid, Onyenegecha Chibueze P. Backward bifurcation and optimal control in a co-infection model for SARS-CoV-2 and ZIKV. Results Phys 2022;37:105481.
- [52] Ringa N, Diagne ML, Rwezaura H, Omame A, Tchoumi SY, Tchuenche JM. HIV and COVID-19 co-infection: A mathematical model and optimal control. Inform Med Unlocked 2022;31:100978.
- [53] Sun Wenyu, Yuan Ya-Xiang. Optimization theory and methods: nonlinear programming, vol. 1, Springer Science & Business Media; 2006.
- [54] Pontryagin L, Boltyanskii V, Gamkrelidze R, Mishchenko E. John wiley & sons; new york/London: 1963. Math Theory Optim Control Process 1962;4.
- [55] Lenhart Suzanne, Workman John T. Optimal control applied to biological models, 5-33. CRC Press; 2007, p. 5-33.
- [56] Kingsley Paul Vijay, Arunkumar Govindakarnavar, Tipre Meghan, Leader Mark, Sathiakumar Nalini. Pitfalls and optimal approaches to diagnose melioidosis. Asian Pacific J Trop Med 2016:9(6):515–24.
- [57] Engida Habtamu Ayalew, Theuri David Mwangi, Gathungu Duncan Kioi, Gachohi John. Optimal control and cost-effectiveness analysis for leptospirosis epidemic. J Biol Dyn 2023;17(1):2248178.
- [58] Hugo Alfred, Makinde Oluwole Daniel, Kumar Santosh, Chibwana Fred F. Optimal control and cost effectiveness analysis for Newcastle disease eco-epidemiological model in Tanzania. J Biol Dyn 2017;11(1):190–209.